iScience

CellPress
OPEN ACCESS

Article

Dissection of the MEF2D-IRF8 transcriptional circuit dependency in acute myeloid leukemia

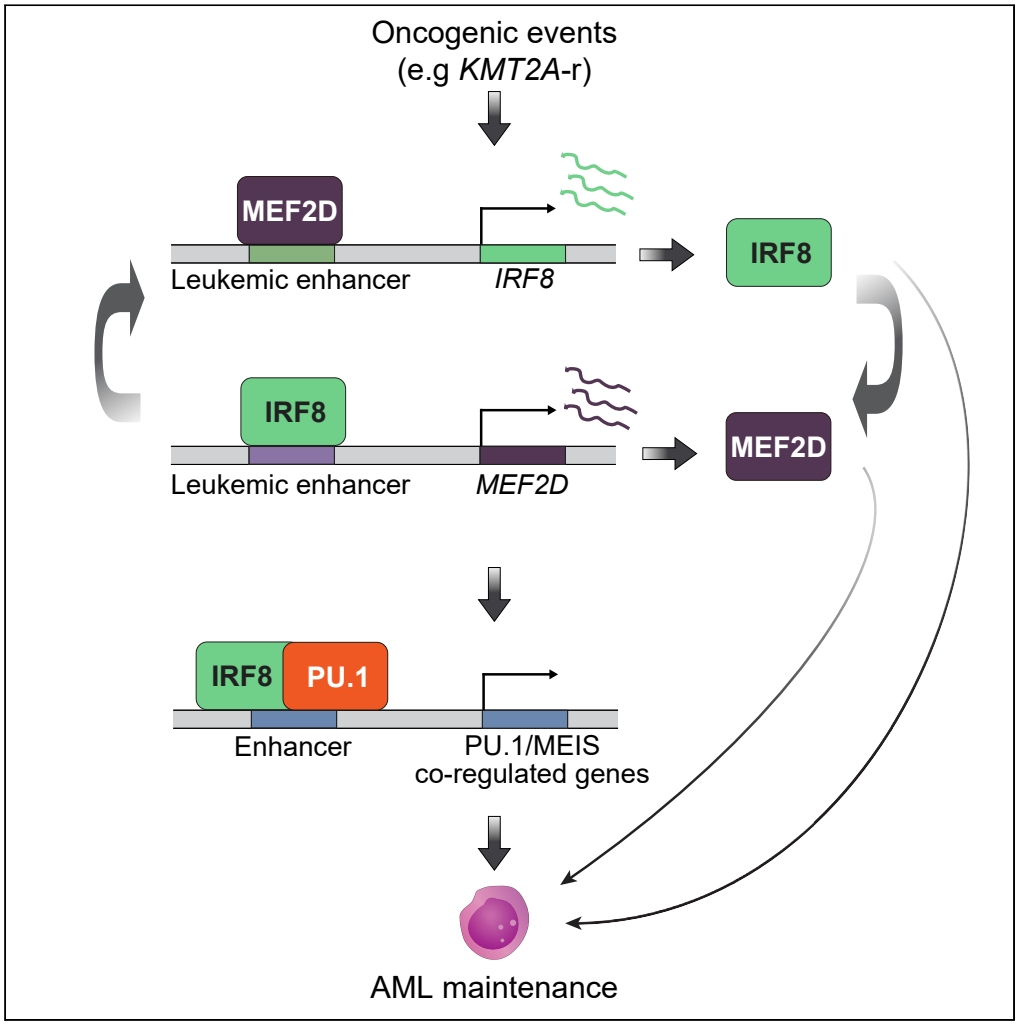

Bianca Y. Pingul, Hua Huang, Qingzhou Chen, ..., Shelley L. Berger, Zhendong Cao, Junwei Shi

zhendon@pennmedicine.upenn.edu (Z.C.)
jushi@upenn.edu (J.S.)

Highlights

MEF2D is a context-specific vulnerability in *IRF8*^{hi} AML

MEF2D and IRF8 form a transcriptional circuit via binding to each other's enhancers

MEF2D-IRF8 circuit supports PU.1's chromatin occupancy and transcriptional output

MEF2D and IRF8 can regulate separate gene expression programs alongside the circuit

Pingul et al., iScience *25*, 105139
October 21, 2022
https://doi.org/10.1016/j.isci.2022.105139

iScience

CellPress
OPEN ACCESS

Article

Dissection of the MEF2D-IRF8 transcriptional circuit dependency in acute myeloid leukemia

Bianca Y. Pingul,[1,2,3,4,9] Hua Huang,[3,5] Qingzhou Chen,[3,4] Fatemeh Alikarami,[6] Zhen Zhang,[3,5] Jun Qi,[7] Kathrin M. Bernt,[6,8] Shelley L. Berger,[3,5] Zhendong Cao,[1,3,4,9,*] and Junwei Shi[1,3,4,10,*]

SUMMARY

Transcriptional dysregulation is a prominent feature in leukemia. Here, we systematically surveyed transcription factor (TF) vulnerabilities in leukemia and uncovered TF clusters that exhibit context-specific vulnerabilities within and between different subtypes of leukemia. Among these TF clusters, we demonstrated that acute myeloid leukemia (AML) with high *IRF8* expression was addicted to *MEF2D*. MEF2D and IRF8 form an autoregulatory loop via direct binding to mutual enhancer elements. One important function of this circuit in AML is to sustain PU.1/MEIS1 co-regulated transcriptional outputs via stabilizing PU.1's chromatin occupancy. We illustrated that AML could acquire dependency on this circuit through various oncogenic mechanisms that results in the activation of their enhancers. In addition to forming a circuit, MEF2D and IRF8 can also separately regulate gene expression, and dual perturbation of these two TFs leads to a more robust inhibition of AML proliferation. Collectively, our results revealed a TF circuit essential for AML survival.

INTRODUCTION

Transcription factors (TFs) encompass one or multiple direct DNA binding domains and represent one of the most important classes of proteins in interpreting eukaryotic genomes. An estimated number of ~1,600 TFs in the human genome are likely to engage DNA in a sequence-specific manner, and many of them are biochemically and functionally obscure (Lambert et al., 2018; Vaquerizas et al., 2009). Although nearly half of these TFs are ubiquitously expressed in all types of cells, a small number of TFs, termed master regulator TFs, are expressed in a cell type specific manner and play fundamental roles in cell fate determination (Buganim et al., 2013; Davis et al., 1987; Graf and Enver, 2009). Master TFs typically form interconnected autoregulatory loops to control each other's expression and their downstream transcriptional programs by coordinately modulating their enhancer activities (Boyer et al., 2005; Lee and Young, 2013). Such transcriptional circuitry enables rapid induction and sustained augmentation of gene expression programs to determine a cell state (Lee and Young, 2013; Young, 2011).

Malignant transformation involves transcriptional dysregulation mediated by the master TF circuitry (Bradner et al., 2017). For example, in acute myeloid leukemia (AML), an aggressive form of cancer characterized by the overproduction of immature myeloid precursor cells, recurrent oncogenic alterations occur in TFs and epigenetic regulators, such as CEBPA, RUNX1, GATA2, and KMT2A (also known as Mixed-Lineage Leukemia 1 (*MLL1*)), which are essential for stem cell renewal and myeloid differentiation (Döhner et al., 2015; Khwaja et al., 2016). A second category of TFs exploited in leukemia is non-oncogenic dependencies, which are not frequently mutated but required for sustaining malignant states, such as FLI1, ERG, and ZFP64 in AML (Lu et al., 2018; Roe et al., 2015; Xu et al., 2018). However, there remains an unmet need for a comprehensive understanding of TF-mediated coordination of gene regulation in cancer, which may ultimately foster the development of effective and selective therapeutic strategies. In this study, we highlight a comprehensive identification of TF clusters in a broad range of leukemias, which consequently may be utilized as predictive markers of context-specific vulnerabilities.

Myocyte Enhancer Factor (MEF2, A-D) proteins are evolutionarily conserved MADS (MCM1, AGAMOUS, DEFICIENS and SRF) TFs implicated in normal muscle, neuron, and blood system cell development, as well as in human diseases (Di Giorgio et al., 2018; Krivtsov et al., 2006; Pon and Marra, 2015; Potthoff and Olson, 2007). Among them, MEF2D is reported to be upregulated in certain types of cancer (Ma

[1]Department of Cancer Biology, Perelman School of Medicine, University of Pennsylvania, Philadelphia, PA 19104, USA

[2]Graduate Group in Biochemistry and Molecular Biophysics, Perelman School of Medicine, University of Pennsylvania, Philadelphia, PA 19104, USA

[3]Epigenetics Institute, Department of Cell and Developmental Biology, Perelman School of Medicine, University of Pennsylvania, Philadelphia, PA 19104, USA

[4]Abramson Family Cancer Research Institute, Perelman School of Medicine, University of Pennsylvania, Philadelphia, PA 19104, USA

[5]Department of Cell and Developmental Biology, Perelman School of Medicine, University of Pennsylvania, Philadelphia, PA 19104, USA

[6]Division of Pediatric Oncology, Children's Hospital of Philadelphia, Philadelphia, PA 19104, USA

[7]Department of Cancer Biology, Dana-Farber Cancer Institute, Department of Medicine, Harvard Medical School, Boston, MA 02215, USA

[8]Department of Pediatrics, Perelman School of Medicine at the University of Pennsylvania and Abramson Cancer Center, Philadelphia, PA 19104, USA

[9]These authors contributed equally

[10]Lead contact

*Correspondence: zhendon@pennmedicine.upenn.edu (Z.C.), jushi@upenn.edu (J.S.)

https://doi.org/10.1016/j.isci.2022.105139

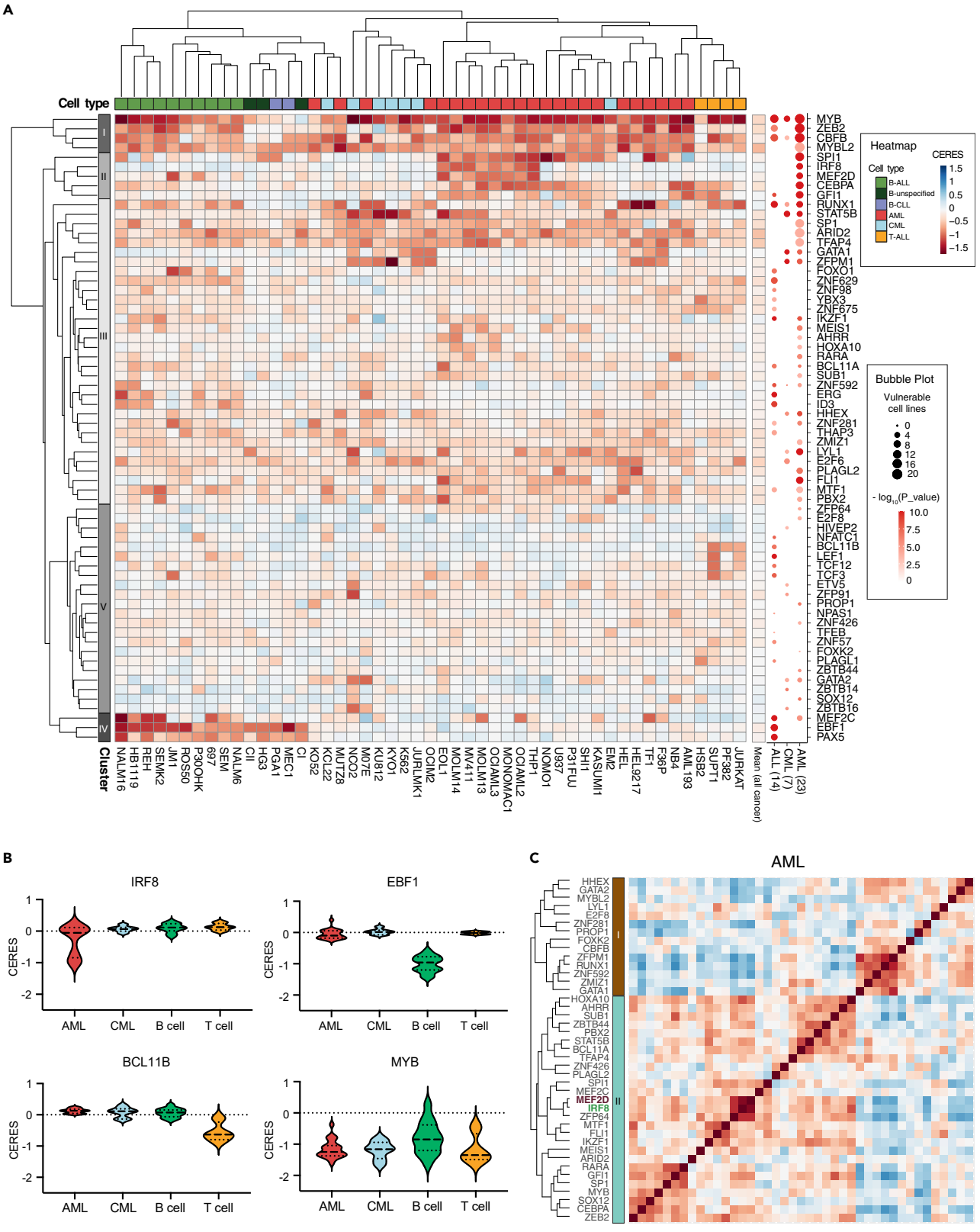
A
Cell type
Heatmap
Cell type
B-ALL
B-unspecified
B-CLL
AML
CML
T-ALL
CERES
1.5
1
0.5
0
−0.5
−1
−1.5
Bubble Plot
Vulnerable cell lines
0
4
8
12
16
20
- log10(P_value)
10.0
7.5
5.0
2.5
0
MYB
ZEB2
CBFB
MYBL2
SPI1
IRF8
MEF2D
CEBPA
GFI1
RUNX1
STAT5B
SP1
ARID2
TFAP4
GATA1
ZFPM1
FOXO1
ZNF629
ZNF98
YBX3
ZNF675
IKZF1
MEIS1
AHRR
HOXA10
RARA
BCL11A
SUB1
ZNF592
ERG
ID3
HHEX
ZNF281
THAP3
ZMIZ1
LYL1
E2F6
PLAGL2
FLI1
MTF1
PBX2
ZFP64
E2F8
HIVEP2
NFATC1
BCL11B
LEF1
TCF12
TCF3
ETV5
ZFP91
PROP1
NPAS1
ZNF426
TFEB
ZNF57
FOXK2
PLAGL1
ZBTB44
GATA2
ZBTB14
SOX12
ZBTB16
MEF2C
EBF1
PAX5
I
II
III
V
IV
Cluster
NALM16
HB1119
REH
SEMK2
JM1
ROS50
P30OHK
697
SEM
NALM6
CII
HG3
PGA1
MEC1
CI
KO52
KCL22
MUTZ8
NCO2
M07E
KU812
KYO1
K562
JURLMK1
OCIM2
EOL1
MOLM14
MV411
MOLM13
OCIAML3
MONOMAC1
OCIAML2
THP1
NOMO1
U937
P31FUJ
SHI1
KASUMI1
EM2
HEL
HEL9217
TF1
F36P
NB4
AML193
HSB2
SUPT1
PF382
JURKAT
Mean (all cancer)
AML (23)
CML (7)
ALL (14)
B
IRF8
EBF1
BCL11B
MYB
CERES
AML
CML
B cell
T cell
C
AML
HHEX
GATA2
MYBL2
LYL1
E2F8
ZNF281
PROP1
FOXK2
CBFB
ZFPM1
RUNX1
ZNF592
ZMIZ1
GATA1
HOXA10
AHRR
SUB1
ZBTB44
PBX2
STAT5B
BCL11A
TFAP4
ZNF426
PLAGL2
SPI1
MEF2C
MEF2D
IRF8
ZFP64
MTF1
FLI1
IKZF1
MEIS1
ARID2
RARA
GFI1
SP1
MYB
SOX12
CEBPA
ZEB2
I
II

Figure 1. Integrative analysis of TF dependency map in leukemia

(A) Heatmap (left) depicts hierarchically clustered dependency scores (CERES) of 66 TFs that are significantly enriched in AML, CML or ALL cell lines. A total of 49 leukemia cell lines with CRISPR screens available on DepMap were plotted. Pan-essential and non-essential genes were excluded. A bubble plot (right) indicates number of cell lines (by size) that are vulnerable (CERES < -0.45) to indicated TF perturbation, where color density represents significant enrichment level. AML, acute myeloid leukemia; CML, chronic myeloid leukemia; ALL, acute lymphoblastic leukemia.

(B) Violin plots of representative TF CERES effects in leukemia.

(C) Pearson correlation matrix of CERES dependency scores of AML-biased TF dependencies. A total 23 AML cell lines were used. Genetic information of cell lines used for this analysis can be found in Table S5.

et al., 2014; Xu and Zhao, 2016), and MEF2D-fusion is a prediction marker for a poor clinical prognosis in B-cell precursor ALL (BCP-ALL) and may be involved in leukemogenesis (Gu et al., 2016a; Liu et al., 2016; Ohki et al., 2019; Suzuki et al., 2016; Tsuzuki et al., 2020). Interferon Regulatory Factor 8 (IRF8), a hematopoietic lineage-specific TF, has been implicated as a key myeloid and B lymphoid cell fate determinator (Holtschke et al., 1996; Lu et al., 2003; Tamura et al., 2015; Wang et al., 2008). Both MEF2D and IRF8 were nominated as AML essential transcriptional vulnerabilities from TF-focused CRISPR screens (Cao et al., 2021; Lu et al., 2018). Mechanistically, we found that an epigenetic reader protein ZMYND8 directly regulates IRF8 transcriptionally and IRF8 regulates MEF2D expression in AML cells. Of interest, our transcriptomic profiling of MEF2D deficient cells revealed that IRF8 could be one of its downstream targets (Cao et al., 2021). However, the essential role of MEF2D in leukemia, whether and how MEF2D maintains IRF8 expression, and why the IRF8-MEF2D network is important for AML remain to be fully investigated.

In this study, we demonstrated that genetic perturbation of *MEF2D* led to robust suppression of cell proliferation in a subset of AMLs with high *MEF2D* expression. On chromatin, we found that MEF2D regulated *IRF8* transcription through occupying an AML-specific *IRF8* enhancer, which eventually formed a positive feedback loop to maintain high *MEF2D* expression. Furthermore, we systematically identified an IRF8-bound intronic enhancer of MEF2D, which we illustrate to have high chromatin accessibility in several patient-relevant genetic alterations such as *KMT2A*-rearrangement. Current models depicting transcriptional circuitries in cancer focus on convergent roles of master TFs in sustaining oncogenic transcriptional programs (Bradner et al., 2017). Here, we found that MEF2D and IRF8 convergently co-regulated a set of genes, and divergently their own respective transcriptional programs to support AML. Mechanistically, the MEF2D-IRF8 circuit functionally supports the transcriptional output of PU.1, and dual perturbation of *MEF2D* and *IRF8* displayed a more profound effect on inhibiting AML proliferation than individual gene perturbation. Together, our results highlighted the coordination between master TFs in the regulation of AML-specific transcriptional program and identified the MEF2D-IRF8 pathway as an AML-specific TF vulnerability.

RESULTS

Integrative analysis of TF dependency map in leukemia identifies distinct TF clusters that exhibit context-specific vulnerabilities

Genome-wide CRISPR-based knockout genetic screens across a broad spectrum of cancer cell lines, such as the DepMap portal, provide rich resources for cancer type-specific vulnerability nominations (Dharia et al., 2021; Tsherniak et al., 2017). To comprehensively annotate leukemia-biased transcriptional vulnerabilities, we surveyed a total of 990 cancer cell lines including 23 AML, 7 chronic myeloid leukemia (CML), 4 T-ALL and 15 B-cell leukemia cell lines. After filtering pan-essential and non-essential genes, we established 66 TFs that displayed leukemia-biased vulnerabilities for further analysis. Unsupervised clustering of their dependency scores (copy-number-adjusted essentiality score, or CERES) (Meyers et al., 2017) nominated five distinct classes of TFs (Figure 1A). Among them, class I, II, and IV displayed the most distinguishable and cancer-type related features. Class I contained TFs that represent a class of blood-lineage specific vulnerabilities, such as *MYB*, *ZEB2*, and *CBFB*, that were essential for proliferation of most leukemia cell lines (Li et al., 2017; Tang et al., 2000; Zuber et al., 2011a) (Figures 1A and 1B). Class II contained TFs, such as *SPI1*, *IRF8*, *MEF2D* and *CEBPA*, that were essential for the proliferation of a subset of AML cell lines, many of which harbor a *KMT2A*-rearrangement or amplification (hereafter called *KMT2A-r* or *KMT2A-amp*, respectively) (Table S5) (Cao et al., 2021; Liss et al., 2021; Ohlsson et al., 2014; Zhou et al., 2014), whereas Class IV included TFs that were required for B cell leukemia proliferation (Figures 1A, 1B, and S1B–S1D). The Class III and V clustering revealed no strong exclusivity of TF dependencies in specific leukemias, but rather a broader requirement pattern across these subtypes. Notable TFs in Class III included GATA1 and STAT5B, which were both essential for AML and CML proliferation, whereas Class V included

TFs such as BCL11B, TCF3, and TCF12 that were more prominently required for T-cell development/T-ALL proliferation (Ha et al., 2017; Kollmann et al., 2019; Shimizu et al., 2008; Staal et al., 2016; Wingelhofer et al., 2018; Zhan et al., 2017) (Figure 1A).

We then interrogated the correlation between TF dependencies within the same subtype of leukemia. Individual hierarchical clustering of CERES in AML, CML and ALL revealed differential dependency profiles of the TF subsets (Figures S1E–S1G). In AML, HOXA10, MEIS1, MEF2C, MYB, ZFP64 and IRF8 are positively associated together. The dysregulation of these TFs are commonly reliant on certain types of AML including those harboring *KMT2A-r* or *KMT2A-amp* (Figure 1C) (Cao et al., 2021; Krivtsov et al., 2006; Lu et al., 2018; Zuber et al., 2011a,2011b). Conversely, RUNX1 and CBFB, which form a heterodimeric complex and were shown to be downregulated in *KMT2A*-r AML (Martinez-Soria et al., 2018; Tang et al., 2000; Zhang et al., 2003; Zhao et al., 2014), were clustered into the second subset. In ALL, B- and T-ALL biased dependencies were well separated, whereas pan-leukemic essential genes such as MYB, RUNX1 and CBFB, tend to correlate with both classes of dependencies (Figure S1E). In CML, we also observed two distinct classes of TFs (Figure S1F), implying that these TFs may be involved in different cellular pathways in the context of BCR-ABL/Ph + leukemia (Wainberg et al., 2021; Wang et al., 2017; Zhang, 2008).

We further assessed the molecular signatures that the 66 leukemia-biased TFs are involved in. Gene Ontology (GO) analysis of the TFs revealed a common signature of significant enrichment of molecular function in enhancer binding and transcription activator, and biological processes such as hematopoietic cell differentiation, T and B cell activation and cell fate commitment (Figure S1G). Using a disease-related gene prioritization tool (Jourquin et al., 2012; Liao et al., 2019), we found that these TFs were predominately enriched for various leukemia types (Figure S1H). These observations suggest that cancer cells are likely to exploit similar, if not the same, transcriptional programs that were primitively utilized by the cell of origin.

MEF2D is an AML-biased dependency

Our integrative TF analysis nominated hits that are not well studied as leukemia dependencies, including ZNF629, YBX3, ZNF98 and ZNF675 in lymphoblastic leukemia, ID3 in B-ALL, and MEF2D, ARID2 and TFAP4 in AML. We focused on MEF2D, a potent and selective vulnerability that has not yet been extensively characterized in a subset of AML (Figures 1 and2A). First, we cloned two independent sgRNAs for MEF2D and confirmed efficient depletion of MEF2D through immunoblotting (Figure S2A). To evaluate the knockout effects of MEF2D, we conducted competition-based proliferation assays in a collection of leukemia cell lines with different cytogenetics. Cas9-expressing cells were partially transduced with sgRNA expression vector linked with GFP, and relative cell growth rate was calculated by tracking the sgRNA positive (GFP positive) population over a time course. Perturbation of MEF2D strongly impaired the growth of AML cell lines, including MOLM-13, MV4; 11 and THP-1 that harbor *KMT2A*-r, as well as OCI-AML3 and OCI-AML5 that carry *DNMT3A/NRAS/NPM1c* or *ASXL1/RUNX1/TET2/EZH2* mutations, respectively, but did not influence the growth of other cancer cell lines, such as K562 JURKAT, OPM1, A375 and HUH7 (Figures 2B, S2B, and S2C).

Moreover, we sought to assess the requirement of MEF2D in normal myeloid cell development. We transduced murine bone marrow cells constitutively expressing Cas9 with sgRNA targeting *Mef2d* (Figure S3D), confirmed the on-target knockout through immunoblotting (Figure S3E), and assessed the development of normal myeloid cells in colony formation assays. We did not observe a significant difference in the frequency and the absolute colony number of hematopoietic progenitor cells on *Mef2d* depletion (Figure S3F). This result is consistent with the notion that loss of Mef2d in a mouse model did not impede normal myeloid cell development (Pattison et al., 2020).

MEF2D has two human isoforms annotated with different Transcription Start Site (TSS). Both isoforms encode almost identical proteins, except one that excludes a small fraction of the *Trans*-activation Domain 2 (TAD2) through alternative splicing (Figure S2G). To verify the on-target effect of the MEF2D sgRNA, we transduced AML cells with CRISPR-resistant MEF2D-long or short cDNA and found that both isoforms were able to fully rescue the growth-arrest phenotype caused by sgRNA-mediated MEF2D inactivation (Figures S2H–S2J). This data suggested a redundant function of the two MEF2D isoforms in AML survival, although AML cell lines and primary patient samples mostly expressed the long isoform, as demonstrated by qPCR and RNA-seq (Figures S2K and S2L). In addition, inspection of cancer cell line encyclopedia (CCLE) dataset (Barretina et al., 2012) revealed a positive correlation between MEF2D's CERES and its mRNA

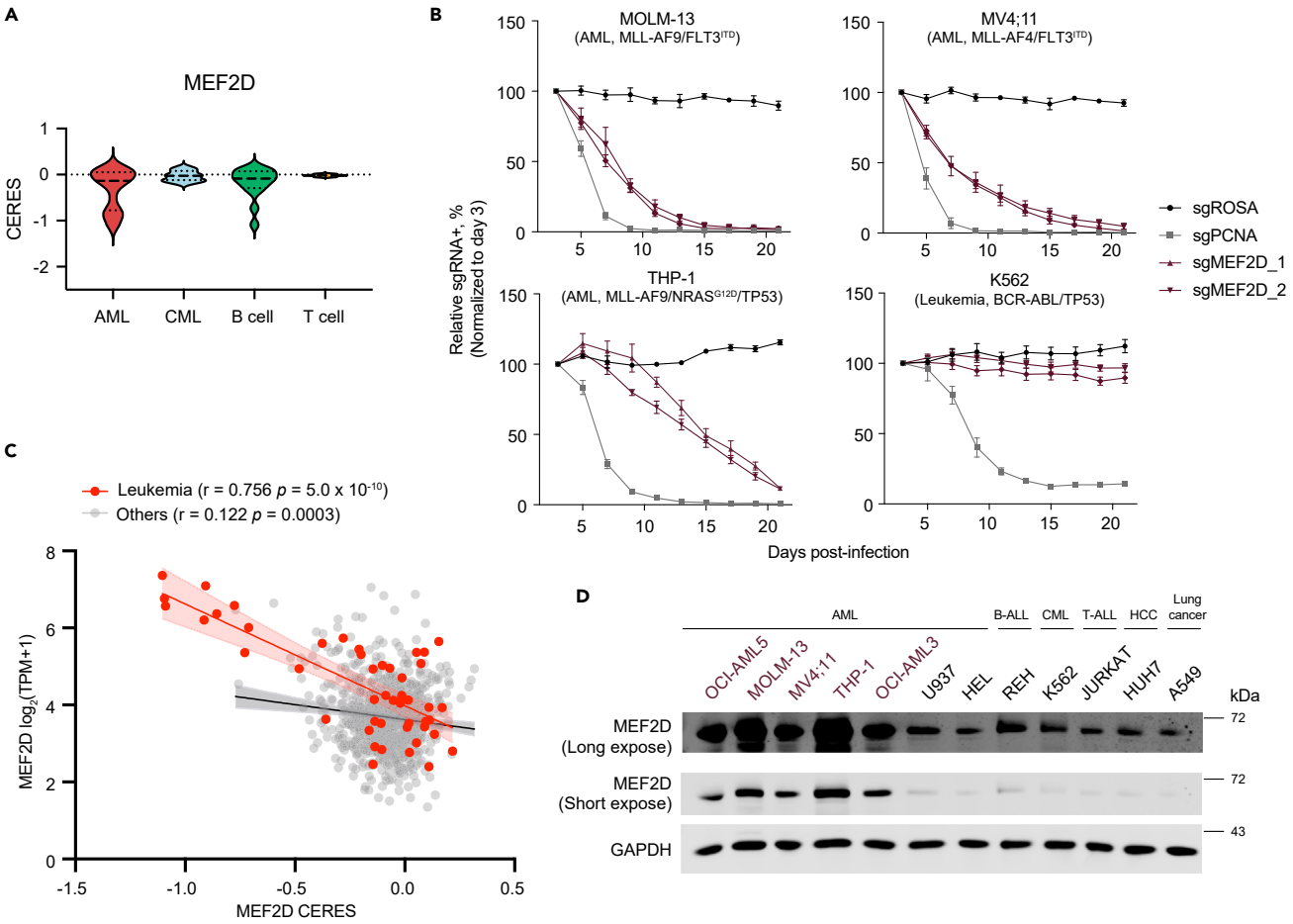

Figure 2. MEF2D is an AML-biased dependency

(A) Violin plots of MEF2D CERES effects.

(B) Competition-based proliferation assays in MOLM-13 (AML, upper left), MV4; 11 (AML, upper right), THP1 (AML, bottom left) and K562 (an acute (erythro) blastic transformation of prior CML, bottom right) cell lines stably expressing Cas9. Plotted are relative GFP/sgRNA + population normalized based on day 3 (n = 3–5, mean ± SEM). sgNeg, negative control. sgPCNA, positive control.

(C) Scatterplot that shows a linear correlation between MEF2D's CERE dependency scores and mRNA expression in leukemia (red) or other cancer cell lines (light gray) in the DepMap dataset. Each dot represents one cell line; the shaded regions indicate 95% confidence interval for the linear regression model.

(D) Immunoblotting of MEF2D in indicated whole-cell lysates. MEF2D^{hi} cell lines are labeled in purple. HCC, Hepatocellular carcinoma.

expression in leukemia cell lines (Figure 2C). We further confirmed by immunoblotting that high expression level of MEF2D protein was associated with MEF2D dependency in a subset of AML (Figure 2D). AML cell lines that were most reliant on MEF2D expressed high levels of MEF2D, whereas cell lines that had a basal level of MEF2D expression did not require MEF2D for their proliferation. Together, our findings validate MEF2D as a TF vulnerability in a subset of AML.

MEF2D and IRF8 form an autoregulatory loop in AML via direct binding of mutual enhancer

We set out to further explore the relationship between the leukemia-biased dependencies and their mRNA expression levels by performing a pair-wise correlation analysis. This analysis revealed that the expression levels of several TF groups were mutually positively correlated with their vulnerabilities in leukemia (Figure 3A). Evaluation of these correlated gene expression profiles may provide a rationale to guide the clinical application of TF pathway focused targeted therapy. For example, the high expression levels of *TFEB*, *PAX5*, *EBF1*, and *FOX O 1* might be able to serve as prediction markers for *EBF1* and *PAX5* dependencies in B-cell leukemia (Figure 3A). Of note, we found that the high expression of a TF group (*MEF2D*, *IRF8*, *HOXA10*, *MEIS1*, *SPI1*, *CEBPA*, *ZEB2*, and *GFI1*) collectively predicted individual members' dependencies

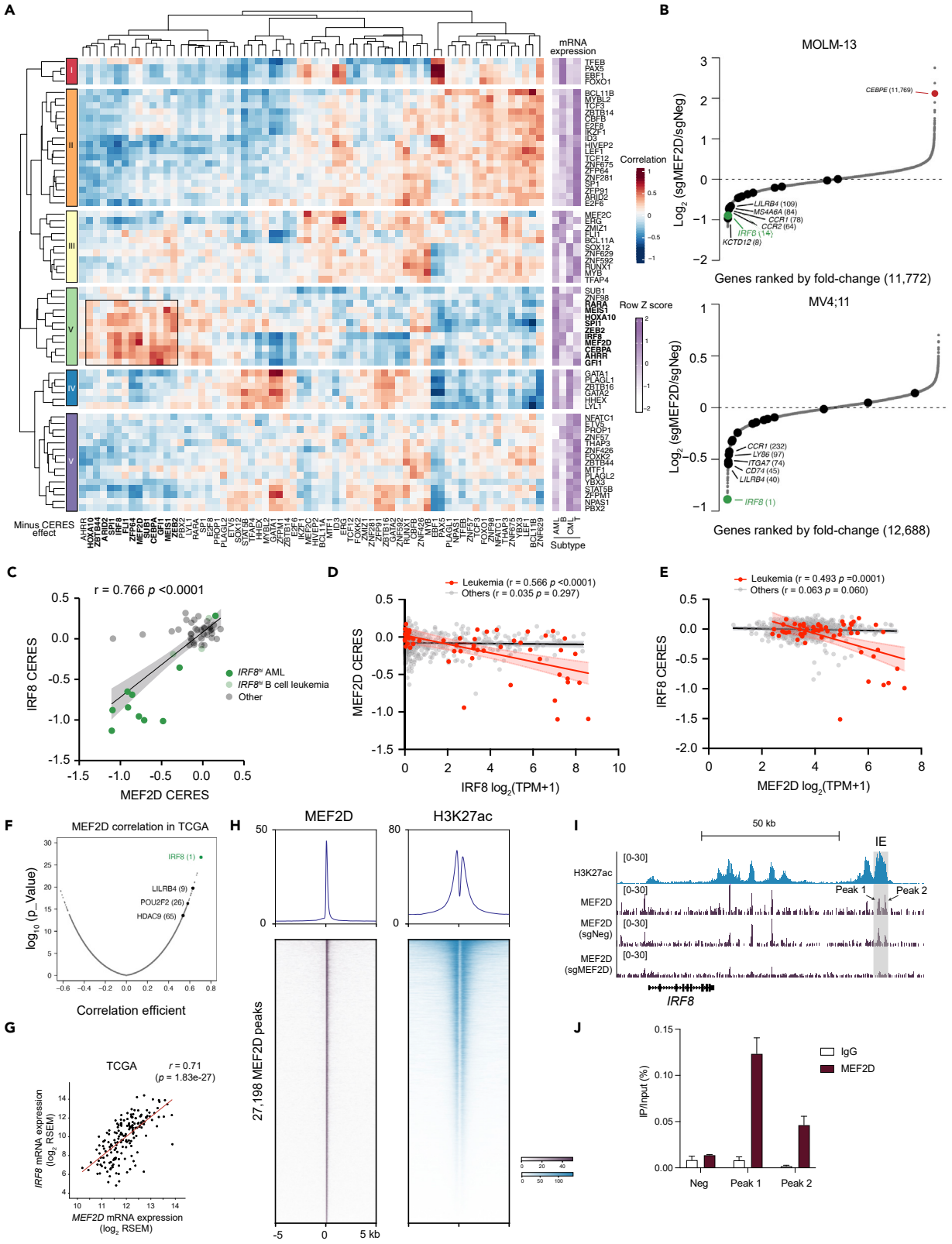
A
mRNA expression
Correlation
Row Z score
Minus CERES effect
Subtype
AML
B ALL
CML
B
MOLM-13
Log2 (sgMEF2D/sgNeg)
Genes ranked by fold-change (11,772)
MV4;11
Log2 (sgMEF2D/sgNeg)
Genes ranked by fold-change (12,688)
C
r = 0.766 p <0.0001
IRF8 CERES
MEF2D CERES
IRF8hi AML
IRF8hi B cell leukemia
Other
D
Leukemia (r = 0.566 p <0.0001)
Others (r = 0.035 p = 0.297)
MEF2D CERES
IRF8 log2(TPM+1)
E
Leukemia (r = 0.493 p =0.0001)
Others (r = 0.063 p = 0.060)
IRF8 CERES
MEF2D log2(TPM+1)
F
MEF2D correlation in TCGA
log10 (p_Value)
Correlation efficient
G
TCGA
r = 0.71
(p = 1.83e-27)
IRF8 mRNA expression (log2 RSEM)
MEF2D mRNA expression (log2 RSEM)
H
MEF2D
H3K27ac
27,198 MEF2D peaks
-5
0
5 kb
I
50 kb
IE
H3K27ac
MEF2D
MEF2D (sgNeg)
MEF2D (sgMEF2D)
Peak 1
Peak 2
IRF8
J
IP/Input (%)
IgG
MEF2D
Neg
Peak 1
Peak 2

Figure 3. MEF2D-IRF8 regulatory loop in AML

(A) Similarity matrix (left) of 66 leukemia-enriched TF dependencies in their (minus) CERES effects (row) versus mRNA expressions (column) hierarchically clustered by pair-wise Pearson correlation in 49 leukemia cell lines. Heatmap (right) implicates average expression level of TFs in different subtypes of leukemia.

(B) RNA-seq rank plot of gene expression changes in MOLM-13 (up, (Cao et al., 2021)) or MV4; 11 cells 4–5 days after transduction of two independent sgNeg or sgMEF2D. Dark dots indicate IRF8-regulated genes in Figure S3A.

(C) Scatterplot of *MEF2D* CERES versus *IRF8* CERES in leukemia cell lines.

(D and E) Scatterplot that shows a linear correlation between IRF8's mRNA expression and MEF2D's CERES dependency scores (D) or MEF2D's mRNA expression and IRF8's CERES dependency scores (E). Each dot represents one cell line; the shaded regions indicate 95% confidence interval for the linear regression model.

(F) Pearson correlation analysis of *MEF2D* mRNA expression with other genes in 173 AML patients. Data retrieved from TCGA dataset.

(G) Scatterplot of *MEF2D* and *IRF8* expression in 173 AML patients.

(H) Meta-profile (top) and density plot (bottom) of MEF2D CUT&RUN and H3K27ac ChIP-seq peaks in MOLM-13 cells. Peaks are ranked by MEF2D CUT&RUN tag counts.

(I) Gene tracks of H3K27ac and MEF2D enrichment at IRF8 locus in MOLM-13 cells. Shadowed in gray is the AML-specific *IRF8* enhancer (IE). (J) CUT&RUN-qPCR against MEF2D on *IRF8* locus (n = 3).

in AML, which may imply a possible interconnection of their regulatory pathways. Among these TFs, we focused on investigating the uncharacterized function of MEF2D in AML.

We previously showed that IRF8 can directly modulate MEF2D expression in AML (Figure S3A), and MEF2D may also regulate IRF8 expression (Cao et al., 2021). We proposed that IRF8 and MEF2D could form a transcriptional circuit, but the direct downstream targets of MEF2D have not yet been investigated. To assess MEF2D-regulated transcriptional programs in AML, we analyzed RNA sequencing (RNA-seq) 4–5 days after CRISPR-mediated *MEF2D* depletion in 3 AML cell lines and a control cell line (K562). We observed a trend of downregulation for *IRF8* and IRF8-regulated genes (defined as downregulated genes on *IRF8* inactivation in 4 AML cell lines, Figure S3A) in *MEF2D*-addicted AML cell lines, but not in K562 cells which do not express *IRF8* (Figures 3B, S3B, and S3C). Furthermore, we did not observe altered expression of other TFs that were grouped together with MEF2D and IRF8. Indeed, MEF2D and IRF8 shared a highly similar dependence pattern in leukemia (Figures 3C and 1A), and mRNA expression of one is highly correlated with the dependency score of the other in leukemia in comparison to other tumors (Figures 3D and 3E). We also retrieved AML patient transcriptomic profiling data from The Cancer Genome Atlas (TCGA) (Cancer Genome Atlas Research Network et al., 2013) and performed correlation analysis between IRF8/MEF2D and other genes. Notably, *MEF2D* mRNA was positively associated with *IRF8* mRNA and IRF8-regulated genes in AML patients, with *IRF8* as the top 1 gene correlated with *MEF2D* (Figures 3F, 3G, and S3D).

To further evaluate the chromatin occupancy of MEF2D and elucidate MEF2D-mediated gene regulation, we performed Cleavage Under Targets and Release Using Nuclease (CUT&RUN) (Skene et al., 2018) in parental MOLM-13 cells as well as cells transduced with either negative control and *MEF2D* targeting sgRNAs. This identified a total of 27,198 high confidence peaks of MEF2D. Genome-wide MEF2D-binding profiling revealed a significant overlap of MEF2D binding sites with the active histone mark H3K27ac. A large proportion of MEF2D sites were in promoters and distal elements that are likely to be *cis*-element (Figures 3H and S3E), consistent with an established role of MEF2D in transcriptional activation (Kim et al., 2008; Liu et al., 2007; Pon and Marra, 2015; Potthoff and Olson, 2007). Deconvolution of the MEF2D-derived sequence showed enrichment of a previously reported Mef2d motif in murine retina, as well as several hematopoietic lineage-specific TF-binding motifs, such as PU.1, FLI1, IRF8 (Figure S3F). Inspection of *IRF8* locus revealed an enrichment of MEF2D signals at the previously identified AML-specific *IRF8* enhancer region (IE) (Cao et al., 2021) in the parental cells or cells transduced with negative control sgRNA, but not cells with *MEF2D* targeting sgRNA (Figure 3I). The enrichment of MEF2D in the IRF8 IE was further validated by CUT&RUN-qPCR (Figure 3J). Furthermore, we utilized a targeted degradation system (Nabet et al., 2018) to allow rapid depletion of MEF2D to evaluate the primary transcriptional changes on MEF2D loss. We established a THP1 AML cell line with a knockout of the endogenous MEF2D and substituted with a $FKBP12^{G36V}$-linked MEF2D cDNA (termed THP1-dMEF2D), which allowed us to rapidly deplete MEF2D on dTAG treatment (Figures S3G–S3I). We performed a time-course analysis of gene expression following dTAG treatment of THP1-dMEF2D cells and observed rapid loss of *IRF8* transcript, but not other known AML oncogenic drivers such as *FLT3* and *MYC* (Figure S3J). Collectively, these results support that MEF2D and IRF8 form a transcriptional circuit and regulate each other directly.

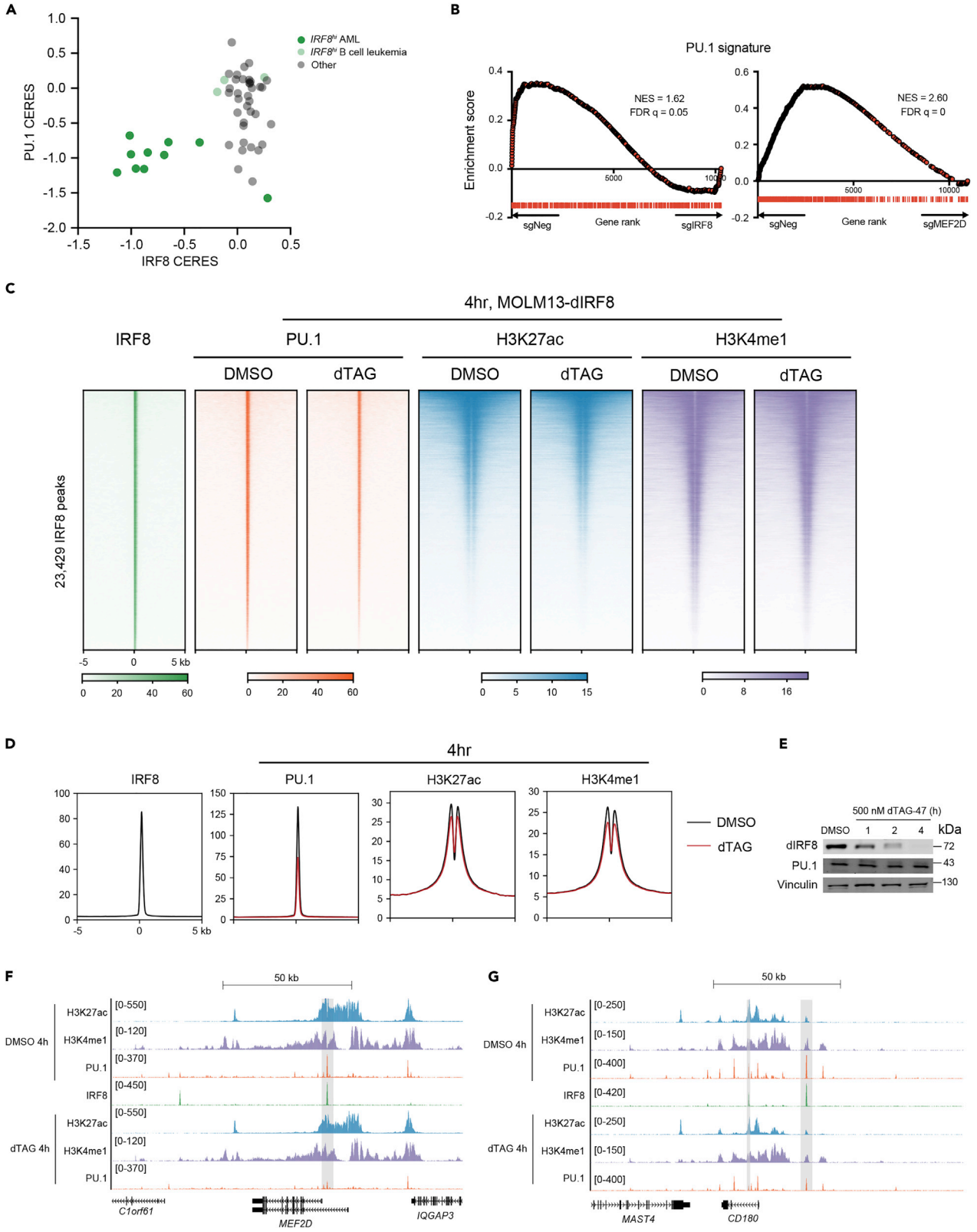
A
PU.1 CERES
IRF8 CERES
IRF8hi AML
IRF8hi B cell leukemia
Other
B
PU.1 signature
Enrichment score
NES = 1.62
FDR q = 0.05
NES = 2.60
FDR q = 0
sgNeg
Gene rank
sgIRF8
sgMEF2D
C
4hr, MOLM13-dIRF8
IRF8
PU.1
H3K27ac
H3K4me1
DMSO
dTAG
23,429 IRF8 peaks
D
4hr
IRF8
PU.1
H3K27ac
H3K4me1
DMSO
dTAG
E
500 nM dTAG-47 (h)
DMSO 1 2 4 kDa
dIRF8
PU.1
Vinculin
F
50 kb
DMSO 4h
dTAG 4h
H3K27ac
H3K4me1
PU.1
IRF8
C1orf61
MEF2D
IQGAP3
G
50 kb
MAST4
CD180

Figure 4. IRF8 supports PU.1's chromatin occupancy and transcriptional output

(A) Scatterplot of *IRF8* CERES versus *PU.1* CERES in leukemia cell lines.

(B) GSEA analysis of IRF8-KO (left) and MEF2D-KO (right) RNA-seq data in MOLM-13 cells. PU.1 signature scatterplot of MEF2D CERES versus IRF8 CERES in leukemia cell lines, where the PU.1 signature is defined as the top 500 downregulated genes on PU.1 depletion. Normalized enrichment score (NES) and false discovery rate (FDR) q value are shown.

(C and D) Density plot (C) and meta-profiles (D) of PU.1, H3K27ac and H3K4me1 ChIP-seq signals at IRF8 binding sites in MOLM13-dIRF8 cells (Cao et al., 2021) on 4 h treatment of DMSO or dTAG that rapidly eliminates IRF8 protein. Peaks are ranked by IRF8 ChIP-seq tag counts (n = 3).

(E) Immunoblotting of IRF8, PU.1 and GAPDH in whole-cell lysates of MOLM13-dIRF8 cells treated with 500nM dTAG-47 for 4h.

(F and G) Gene tracks of ChIP-seq signal from Figures 4C and 4D at *MEF2D* (E) or *CD180* (F) locus.

IRF8 supports PU.1's chromatin occupancy and transcriptional output

To date, the underlying role of the MEF2D-IRF8 circuit in AML maintenance and the subsequent consequences of its activation have not yet been characterized. Previous studies reveal that IRF8 or its homologous protein IRF4 physically associates with PU.1, a master myeloid TF, on a composite DNA element (Eisenbeis et al., 1995; Tamura et al., 2015). IRF8 and PU.1 have also been suggested to play a tumor suppressive role in B cells, and that deletion of IRF8 and PU.1 led to B-ALL development in mice (Pang et al., 2016). In contrast to B-ALL, either genetic or chemical inhibition of PU.1 decreases *KMT2A*-r AML proliferation, partially because of the crosstalk between PU.1 and HOX/MEIS transcriptional programs (Antony-Debré et al., 2017; Zhou et al., 2014). These observations were in concert with the consequence of CRISPR-mediated PU.1 perturbation in leukemia, where PU.1 is essential for IRF8-dependent AML cell lines, but not B cell leukemia (Figure 4A and1A). Of note, PU.1 displayed a broader dependence across AML in comparison to IRF8, which may be because of PU.1's ability to cooperate with other cell-type specific TFs, such as IRF4, CEBPα and RUNX1, for transcriptional regulation (Gu et al., 2018; Zhang et al., 1996) (Figures 1A and S1A).

To evaluate whether IRF8 was functionally connected with PU.1 for gene regulation in AML, we performed transcriptomic profiling in MOLM-13 cells transduced with two independent sgRNAs targeting the DNA-binding domain of PU.1. Efficient PU.1 depletion was confirmed by immunoblotting (Figure S4B). Differential gene expression analysis revealed that loss of PU.1 resulted in the reduction of IRF8-regulated genes, but not *IRF8* mRNA level (Figure S4C). A PU.1 gene signature was defined using the top 500 downregulated genes in AML with PU.1 depletion (Table S1), and gene set enrichment analysis (GSEA) showed a significant downregulation of PU.1 gene signature in both IRF8- and MEF2D-deficient AML cells, but not in K562 (Figures 4B, S4D, and S4E). Because we did not observe changes in PU.1 mRNA levels on IRF8 or MEF2D depletion, it raised a possibility that the transcriptional connection between PU.1 and the MEF2D-IRF8 transcriptional circuit might be mediated through protein-protein interaction on chromatin.

Previous studies suggest that IRF8 directs the monocyte- and dendritic cell (DC)-specific enhancer landscape establishment that are enriched for PU.1 during myeloid cell specification (Kurotaki et al., 2018; Tamura et al., 2015). Therefore, we sought to test whether IRF8 was required for PU.1 binding in AML. We utilized a previously established MOLM13-dIRF8 cell line that allowed rapid and efficient degradation of IRF8 within 1 h via the dTAG system (Cao et al., 2021). We treated the MOLM13-dIRF8 cells with 500 nM dTAG compound and performed ChIP-seq on PU.1, as well as histone markers H3K27ac and H3K4me1 that mark active *cis*-elements. Rapid elimination of IRF8 induced dramatic reduction of PU.1 signals at IRF8-binding sites, whereas H3K27ac, H3K4me1, and the total cellular PU.1 levels were largely unchanged (Figures 4C–4E). Furthermore, extended exposure to dTAG for 24 h only led to a very modest reduction of the H3K27ac and H3K4me1 marks (Figures S4F and S4G). Reduction of PU.1 binding was observed at the loci of *MEF2D* as well as other IRF8-regulated genes *LY86* and *CD180* (Figures 4F, 4G, S4H–S4J). Both *LY86* and *CD180* were implicated to be co-regulated by PU.1 and MEIS1, and were identified as leukemic stem cell markers in chemotherapy-resistant primary AML samples (Saito et al., 2010). These IRF8-dependent PU.1-enriched loci may be unique in these AML subtypes, as the PU.1 signals were stronger in the MOLM-13 and THP-1 cells in comparison to the U937 leukemia cells that harbored CALM-AF10 fusion and expressed low levels of both *MEF2D* and *IRF8* (Figures 2D and S4H–S4J) (Minderjahn et al., 2020; Mohaghegh et al., 2019). These findings are consistent with the structural basis of PU.1/IRF/DNA ternary complex, where PU.1 and IRF4 engage on DNA in a cooperative manner, and this engagement relies on mutual protein-protein interactions (Escalante et al., 2002). To further analyze the cooperative interaction between IRF8 and PU.1, we surveyed IRF8- and PU.1-only sites and found that both these two types of regions had less active histone markers (H3K27ac and H3K4me1) in comparison to IRF8-PU.1 co-occupied regions (Figures S5A and S5B), implying that the IRF8- and PU.1-only sites tend to be less active in terms of

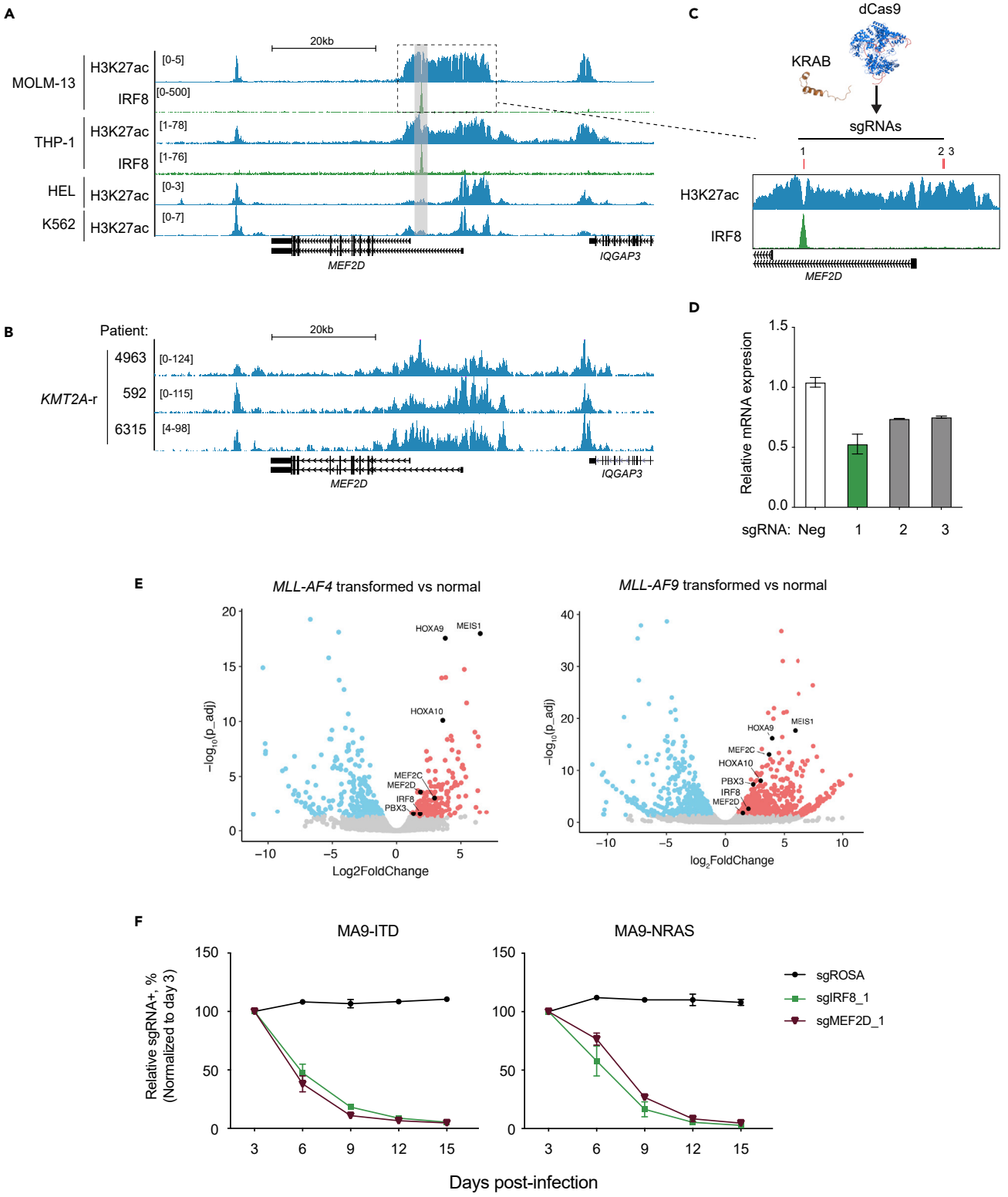

Figure 5. MEF2D and IRF8 are upregulated in AML carrying *KMT2A*-r through enhancer reactivation

(A) Gene tracks of H3K27ac and IRF8 ChIP signals in MOLM-13, THP-1, HEL or K562 cells.

(B) Gene tracks of H3K27ac CUT&RUN signals in primary AML cells, with the key oncogenic mutations labeled on the left.

(C) Schematic of CRISPRi (KRAB-dCas9)-mediated epigenomic silencing at *MEF2D* locus. Red bars indicate sgRNA positions.

Figure 5. *Continued*

(D) RT-qPCR analysis of mRNA expression of *MEF2D* in MOLM-13 cells stably expressing dCas9-KRAB and transduced with indicated sgRNAs in Figure 5B harvested on 4 days post-infection. Relative mRNA levels were normalized to GAPDH levels. Plotted are the mean ± SEM (n = 3 for negative controls, n = 2 for MEF2D sgRNAs).

(E) Volcano plots of RNA-seq data in *MA4*- (left) or *MA9*- (right) transformed human $CD34^+$ HSPCs versus normal HSPCs isolated from BM, where *KMT2A* translocation was induced via CRISPR-Cas9 (Secker et al., 2020).

(F) Competition-based proliferation assays in MA9-$FLT3^{ITD}$ (left) or MA9-$NRAS^{G12D}$ (right) cells, which were generated by retroviral transduction of KMT2A-AF9 followed by FLT3 $FLT3^{ITD}$ and $NRAS^{G12D}$ into human $CD34^+$ HSPC cells, respectively (Wei et al., 2008; Wunderlich et al., 2013) (n = 3, mean ± SEM).

gene transcription and enhancer function in AML. On dTAG-induced IRF8 depletion, we noted that PU.1 was preferentially lost in the IRF8-PU.1 co-occupied regions, as well as that slight loss of PU.1 in some of the PU.1-only regions (Figure S5C). We further confirmed these observations by performing ChIP-qPCR of eight representative genetic loci (Figure S5D). Collectively, these results suggest that the disassociation of PU.1 from IRF8-binding sites is an immediate event on IRF8 depletion, and loss of this interaction leads to suppression of PU.1-specific transcriptional programs required for AML proliferation.

MEF2D and IRF8 are upregulated in AML carrying *KMT2A*-r through enhancer reactivation

Our previous study indicates that *MEF2D* and *IRF8* are upregulated in AML patients with different cytogenetics, and an enhancer-based *IRF8* transcription activation is largely mediated by IE (Cao et al., 2021). Deletion of the homologous murine IE specifically decreased *Irf8* expression in myeloid cells and induced loss of DCs and accumulation of $Ly6C^+$ monocytes (Murakami et al., 2021), suggesting that cancer cells can hijack cell-type specific enhancers to sustain their dysregulated transcriptional network (Bahr et al., 2018; Shi et al., 2013). We surveyed the epigenetic profiles at the *MEF2D* locus and observed a spreading of H3K27ac-enriched and IRF8-bound region to ~10kb downstream of the *MEF2D* long isoform TSS in MOLM-13 and THP-1 cells, both of which were *KMT2A*-r AML with high *IRF8* expression (Figure 5A). In contrast, we observed that H3K27ac signals were more constrained around the TSS of *MEF2D* in both HEL and K562 leukemia cells that were *KMT2A*-WT with no *IRF8* expression (Figure 5A). To further confirm this observation, we performed H3K27ac CUT&RUN in primary patient samples with *KMT2A-r* and noted a similar H3K27ac spreading at the *MEF2D* locus (Figure 5B). Inspection of DNase-seq (Assi et al., 2019) and ATAC-seq (Corces et al., 2016) dataset in AML patients, we observed that a differential chromatin accessibility of the IRF8-bound *MEF2D* intronic enhancer in comparison with the constitutively accessible regions at the TSS of the MEF2D long isoform (Figures S6A and S6B). In normal myelopoiesis, this IRF8-bound *MEF2D* region was transiently activated in granulocyte monocyte progenitor (GMP) in correspondence to an elevated MEF2D expression, whereas the *MEF2D* TSS region was constitutively accessible across the myeloid lineages (Figures S6C and S6D). This observation implied that this cell-state-specific *MEF2D* regulatory element might be hijacked by certain oncogenic drivers during leukemia pathogenesis. To functionally verify the potential regulatory element of *MEF2D*, we employed CRISPR interference (CRISPRi) (Fulco et al., 2016; Gilbert et al., 2013) to silence the H3K27ac-enriched regions at *MEF2D* locus in MOLM-13 cells (Figure 5C). We found that the sgRNA#1 targeting the IRF8-bound site caused a more profound inhibition of *MEF2D* transcription in comparison to the sgRNAs targeting the constitutively active *MEF2D* TSS region (Figures 5A–5D). To further evaluate the functionality of these newly identified enhancer elements, we utilized the optimized opAsCas12a system (Gier et al., 2020) to introduce multiple guide RNAs to the flanking regions of either the IRF8-bound site at *MEF2D* locus or MEF2D-bound site at *IRF8* locus (Figures S6E and S6F). In both scenarios, we observed a mutual and simultaneous reduction of both *IRF8* and *MEF2D* expressions (Figure S6G).

Given the observation that the MEF2D-IRF8 circuit was frequently upregulated in AML cell lines and primary patient samples carrying *KMT2A*-r, we then evaluated whether *KMT2A*-r oncogene itself was sufficient to activate this circuit. We first inspected the public ChIP-seq/CUT&RUN dataset of KMT2A protein and its associated histone H3K79me2 mark (Krivtsov et al., 2019) in MOLM-13 cells and observed both signals at *MEF2D* and *IRF8* loci (Figures S6H and S6I). Next, we surveyed three additional independent datasets, which profiled transcriptomic changes of *KMT2A/MLL-AF9* (MA9) or *KMT2A/MLL-AF4* (MA4)-transformed human $CD34^+$ HSPCs (Horton et al., 2013; Secker et al., 2020) or model leukemias (Barabé et al., 2017), and observed consistent elevation of *MEF2D* and *IRF8*, along with other well-known *KMT2A* target genes *HOXA*, *MEIS1* and *PBX3* (Figure 6E, S6J, and S6K). In pediatric MA9 AML that tends to have much lower mutational burdens (Barabé et al., 2017; Dharia et al., 2021; Gröbner et al., 2018; Ma et al., 2018), *MEF2D* and *IRF8* upregulation was also observed (Figure S6K). Furthermore, CRISPR perturbation of either *IRF8* or *MEF2D* in two MA9-immortalized human $CD34^+$ cell models, with either containing cooperative oncogenic $FLT3^{ITD}$ or $NRAS^{G12D}$ mutations, led to a potent proliferation inhibition (Figures 5F and S6L). Of note, *Flt3-ITD* and *Npm1c* mutations were shown to synergistically rewire chromatin contacts at the

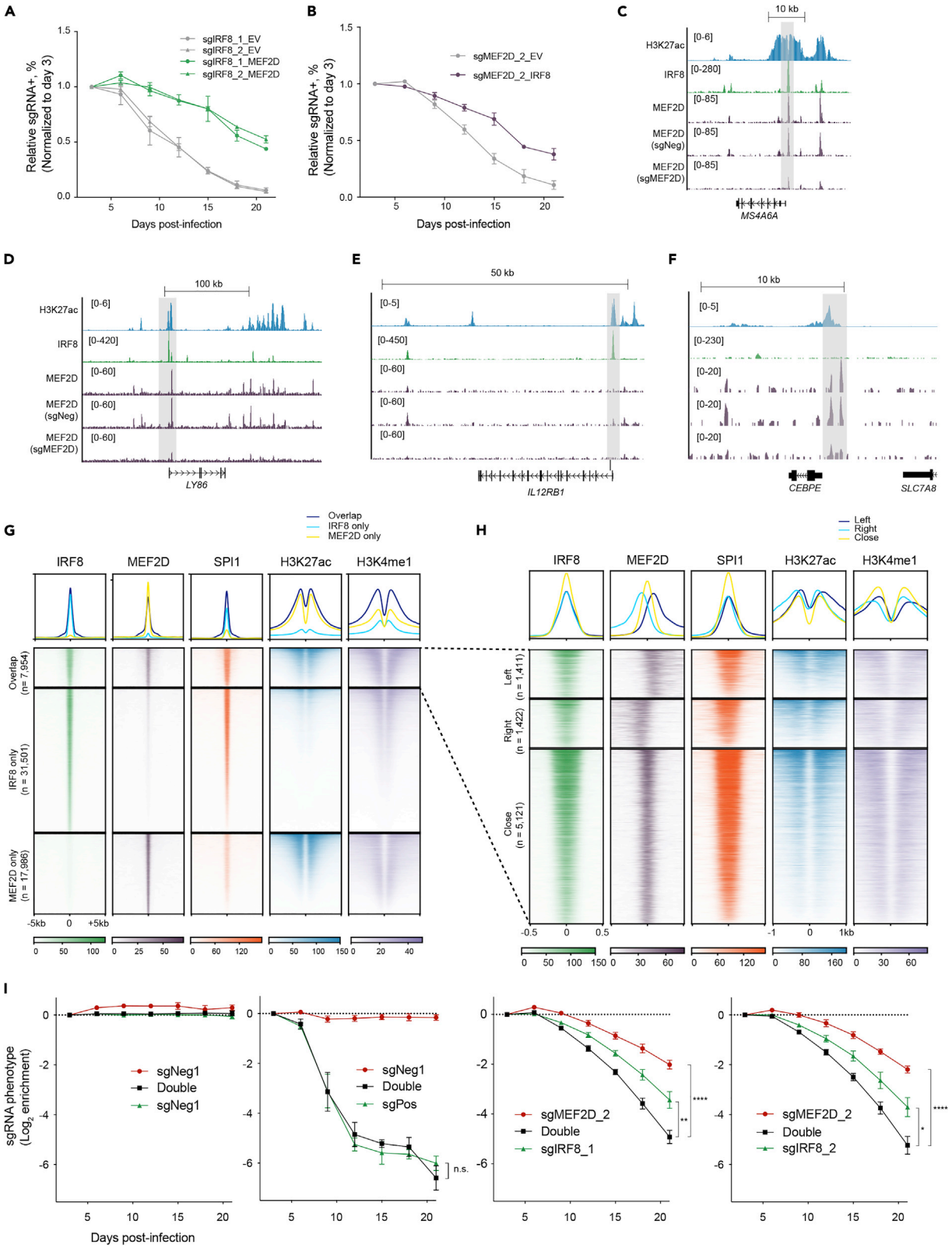
A
Relative sgRNA+, %
(Normalized to day 3)
sgIRF8_1_EV
sgIRF8_2_EV
sgIRF8_1_MEF2D
sgIRF8_2_MEF2D
Days post-infection
B
Relative sgRNA+, %
(Normalized to day 3)
sgMEF2D_2_EV
sgMEF2D_2_IRF8
Days post-infection
C
10 kb
H3K27ac
IRF8
MEF2D
MEF2D (sgNeg)
MEF2D (sgMEF2D)
MS4A6A
D
100 kb
H3K27ac
IRF8
MEF2D
MEF2D (sgNeg)
MEF2D (sgMEF2D)
LY86
E
50 kb
IL12RB1
F
10 kb
CEBPE
SLC7A8
G
Overlap
IRF8 only
MEF2D only
IRF8
MEF2D
SPI1
H3K27ac
H3K4me1
Overlap (n= 7,954)
IRF8 only (n = 31,501)
MEF2D only (n = 17,986)
-5kb
0
+5kb
H
Left
Right
Close
Left (n = 1,411)
Right (n = 1,422)
Close (n = 5,121)
I
sgRNA phenotype (Log2 enrichment)
sgNeg1
Double
sgNeg1
sgNeg1
Double
sgPos
n.s.
sgMEF2D_2
Double
sgIRF8_1
****
**
sgMEF2D_2
Double
sgIRF8_2
****
*
Days post-infection

Figure 6. Divergent function of MEF2D- and IRF8- regulated programs in supporting AML

(A) Competition-based proliferation assays in THP-1 cells transduced with EV or MEF2D cDNA (n = 3–4, mean ± SEM).

(B) Competition-based proliferation assays in THP-1 cells transduced with EV or IRF8 cDNA (n = 3–4, mean ± SEM).

(C–F) Exemplary tracks of genes where MEF2D and IRF8 exact overlap (C), bind in proximity with each other (D), or only IRF8 (E) or MEF2D (F) are enriched.

(G) Meta-profile (top) and density plot (bottom) of IRF8, MEF2D, SPI1, H3K27ac and H3K4me1 enrichment at IRF8-MEF2D co-bound, IRF8-only and MEF2D-regions in MOLM-13 cells. Peaks are ranked by IRF8 or MEF2D tag counts.

(H) Meta-profile (top) and density plot (bottom) depicting detailed classification of IRF8-MEF2D co-bound regions: close, IRF8 and MEF2D peaks have at least 1bp overlap; left, IRF8 binds upstream and MEF2D downstream of the chromosome; right, IRF8 binds downstream and MEF2D upstream of the chromosome. IRF8, MEF2D, SPI1, H3K27ac and H3K4me1 enrichment were plotted. Peaks are ranked by IRF8 tag counts and centered by IRF8 peaks.

(I) Competition-based proliferation assays in THP-1 cells simultaneously transduced with two indicated sgRNAs linked with GFP or mCherry, which produced a mixed population of uninfected, single, and double infected cells. Relative fluorescent (GFP+/cherry+, GFP+/cherry-, GFP-/cherry+) proportion of a single or combinatorial sgRNA was normalized with uninfected cells as an internal control, and the normalized ratios were further compared with that on day 3 to calculate the enrichment of each population (y-axis). sgPos + sgNeg group showed the genome editing was not compromised when two sgRNAs were applied, and no additive/synergistic effect was seen in this combination. (n = 3 for infection with positive and negative controls, n = 5–8 for sgIRF8+ sgMEF2D, mean ± SEM. n.s, not significant; *p < 0.05; **p < 0.01; ****p < 0.001, two-tailed Welch's unpaired t-test).

Irf8 locus and upregulate *Irf8* expression (Yun et al., 2021). Together, these results imply that dependency on the MEF2D-IRF8 transcriptional circuit can be attributed to different leukemia-driving events that converge on altering the epigenetic state of the *MEF2D* and *IRF8* loci.

Divergent function of MEF2D- and IRF8- regulated programs in supporting AML

MEF2D and IRF8 form a transcriptional circuit to control shared downstream genes in supporting AML survival, but it remains unclear whether there are divergent functions of MEF2D and IRF8 in AML. To test this, we investigated whether forced overexpression of either MEF2D or IRF8 was sufficient to rescue each other's deficiency-induced growth defect in AML. Notably, our results demonstrate that ectopic overexpression of either MEF2D or IRF8 in this circuit was able to partially alleviate, but not fully rescue, the growth-arrest phenotype following inactivation of the other in AML, whereas their ectopic overexpression failed to alleviate the growth-arrest phenotype induced by inactivating a pan-essential gene *PCNA* (Figures 6A, 6B and S7A–S7D). Collectively, these data suggested that MEF2D and IRF8 functioned convergently and divergently in supporting AML.

To investigate the divergent function of MEF2D- and IRF8- regulated programs, we examined their chromatin occupancies in AML. Closer inspection of genes enriched for MEF2D and IRF8 binding revealed co-regulated downstream targets (Figures 6C and 6D) and individually regulated genes by MEF2D and IRF8, respectively (Figures 6E and 6F). We noted that MEF2D and IRF8 co-occupied at many of the IRF8-regulated genes (Figures 6C and 6D), which suggested that MEF2D might cooperatively regulate IRF8-targeted genes. We noted that these MEF2D and IRF8 co-occupied regions displayed two distinct patterns: 1) exact overlap with IRF8 peaks, and 2) not exactly at, but in proximity with IRF8 peaks (Figures 6C and 6D). Of note, the MEF2D-only regions included *CEBPE* gene, which has been implicated in myeloid differentiation and immune function (Shyamsunder et al., 2019; Yamanaka et al., 1997) and were upregulated on either *IRF8* or *MEF2D* depletion (Cao et al., 2021) (Figures 3B and S3B).

To further explore their relationship globally, we performed genome-wide co-occupancy analysis of MEF2D and IRF8. We first counted two peaks as overlap when their peak summit positions are 500 bp or less apart and identified 7,954 sites that were co-occupied by these two TFs, and 79.8% of IRF8-enriched and 69.3% of MEF2D-enriched regions were not bound by the other (Figure 6G). As expected, IRF8 was accompanied by PU.1 regardless of MEF2D binding, and unique MEF2D-enriched regions were not positively associated with high PU.1 signals. Notably, IRF8/PU.1/MEF2D co-occupied regions conferred the highest active marks. Alongside, IRF8/PU.1-only regions were weakly enriched for both H3K27ac and H3K4me1, and MEF2D-only regions correlated with low H3K4me1 but comparable H3K27ac with those bound by all the three TFs, implying that these regions may not converge as enhancers but possibly as other types of regulatory elements. Within the overlap of MEF2D-IRF8 pairs, a substantial number (around 40%) were larger than 61 bp (Figure S7E). We further classified the overlap regions based on the proximity of MEF2D peaks in accordance with whether IRF8 peaks are within (close) or over 61bp distance upstream (left) or downstream (right) (Figure S7E). Meta-profiles and density plots revealed 35.6% of the overlap regions fell into the left or right subsets. Strikingly, we also observed a correlation of the overlap regions with the H3K27ac active marks, wherein the enrichment of H3K27ac tended to enclose the MEF2D binding sites. This may suggest that the overlap between MEF2D and IRF8 shifts in correspondence to extended active marks in chromatin.

Considering that MEF2D and IRF8 not only form a transcriptional circuit to control gene expression convergently but also regulate their perspective genes expression programs divergently, we hypothesized that dual inactivation of *MEF2D* and *IRF8* can further suppress leukemia cell proliferation in comparison to individual inactivation. To test this, we simultaneously transduced AML cells with sgMEF2D and sgIRF8 linked with different fluorescence reporter markers (GFP or mCherry), which produced a mixed population of non-infected, single, and dual color cells. Relative growth rates were monitored by the fluorescence percentage normalized to the non-infected control. Indeed, we observed a more severe growth defect in the cell population that received both MEF2D- and IRF8- targeting sgRNAs, in comparison to all the combinations with other sgRNAs (Figures 6I and S7F), which was consistent with the notion that MEF2D and IRF8 had both convergent and divergent functions that are essential for AML proliferation.

DISCUSSION

AML originates from immature hematopoietic cells. During leukemic transformation, cells undergo sporadic but continuous mutations which consequently lead to clonal diversification and heterogeneity (Li et al., 2016). Indeed, these mutational heterogeneities are starkly illustrated in our analysis of TF dependencies in leukemia, which highlighted differential, even opposite requirements between TFs in different subtypes of AML. Therefore, identification of the hallmarks for each subtype of AML, such as driver mutations, chromatin state, and marker gene expression, is critical for targeted therapeutic discovery. Our study mainly focuses on a subset of TFs composed of the MEF2D-IRF8 circuit and certain myeloid TFs, whose high expression levels indicate their vulnerabilities in AML, which can then be exploited for guiding future therapeutic development.

Our previous study on IRF8's role in sustaining AML observes IRF8 directly binding to the *MEF2D* locus and suggests that IRF8 and MEF2D form a transcriptional circuit. Thus, our current study sought to delineate the functional role of MEF2D in this TF circuit and investigate the convergent role of this circuit, as well as whether MEF2D's role differentiates from that of IRF8 in AML maintenance. In addition, the acquisition of dependence on this circuit and its immediate functional output were previously unknown. Here, we leveraged comprehensive approaches to extensively demonstrate the essential role of MEF2D in AML, functionally characterized a patient-relevant intronic enhancer of MEF2D and uncovered the formation of the MEF2D-IRF8 circuit via binding to mutual enhancer element. To date, recent studies revealed the essential roles and activation of MEF2D in AML carrying *KMT2A*-r, and different mechanisms underlying AML maintenance by MEF2D were proposed, including inhibition of CEBPE-mediated myeloid differentiation program, and direct regulation of MYC and HOXA9, which is largely redundant with its homolog TF MEF2C (Harada et al., 2022; Zhao et al., 2021). Although our model suggests the IRF8-MEF2D circuit and MYC program function in parallel in AML, we cannot entirely rule out the context- and cell type-specific roles of MEF2D. Thus, these findings can be complementary to our study and further explain the non-redundant function of MEF2D to IRF8. In line with Harada et al. (2022) highlighting the importance understanding the mechanism by which the IRF8/MEF2D TF circuit is activated, we found that AML carrying certain types of mutations, such as *KMT2A*-fusion and *FLT3*^{ITD} and *NPM1c* cooperating mutations (Yun et al., 2021), can subsequently activate the MEF2D-IRF8 circuit and consequently require it for AML maintenance. To date, the concerted interaction on chromatin between IRF8 and PU.1 has not yet been shown in cellular context. We deciphered the cooperation of IRF8 with PU.1 to specifically sustain essential PU.1/MEIS1 co-regulated transcriptional programs in AML (Zhou et al., 2014). These transcriptional programs may be reinforced by both the MEF2D-IRF8 circuit and an independent MEF2D regulatory function (Figure 7), which could attribute to the enhanced proliferation arrest when MEF2D and IRF8 are simultaneously disrupted.

Previous studies using murine models showed that loss of *Irf8* in mice causes a CML-like syndrome (Holtschke et al., 1996), and can facilitate development of acute promyelocytic leukemia (APL) in cooperation with *PML-RARA* fusion (Gaillard et al., 2018). Minimal reduction of PU.1 and downregulation of *Irf8* are important events for preleukemic stem cell induction in mice with impaired DNA mismatch repair capacity (McKenzie et al., 2019; Will et al., 2015). In contrast to their reported tumor suppressive-like roles, we and others demonstrate that a subset of AMLs are dependent on IRF8 and PU.1 (Antony-Debré et al., 2017; Cao et al., 2021; Gozdecka et al., 2018; Liss et al., 2021; Yun et al., 2021; Zhou et al., 2014). We reason that the differential function of IRF8 and PU.1 in leukemia may be attributed to the cellular contexts and oncogenic mutations, which is supported by our leukemia dependency analysis. In addition, the anti- and pro-tumor activities in AML may also be influenced by the expression level of the TF, because precise regulation of myeloid TF concentration is critical for HSC and leukemic stem cell (LSC) development (Rosenbauer et al., 2005). This idea is supported by a recent study showing that too much or too little EWS-FLI1

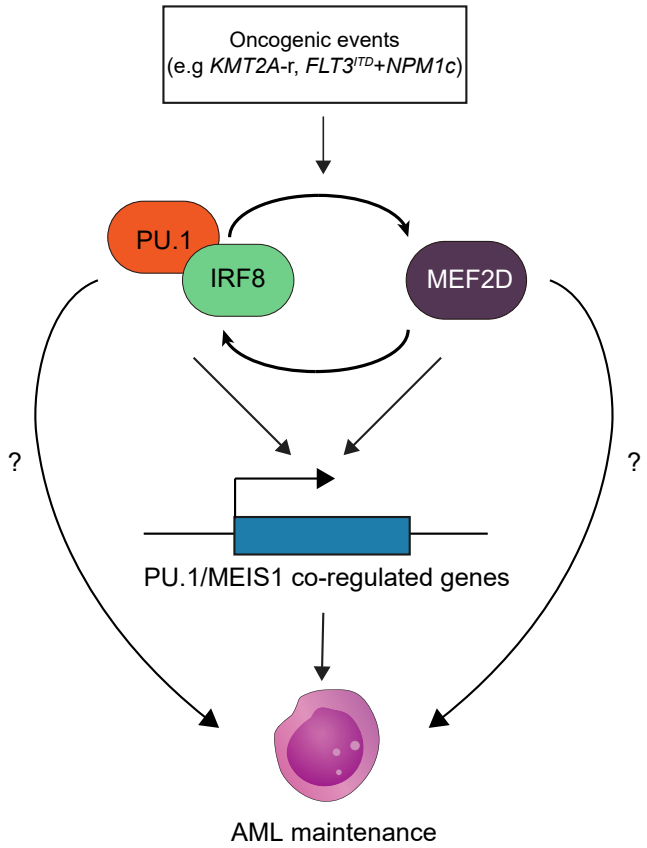

Figure 7. A working model illuminating MEF2D-IRF8 circuit in AML

Oncogenic events (such as *KMT2A-r* and *FLT3*^{ITD} + *NPM1c*) (Yun et al., 2021) can lead to activation and addiction to the MEF2D-IRF8 transcriptional circuit in AML. IRF8-PU.1 complex and MEF2D cooperatively maintain PU.1/MEIS1 co-regulated gene expression (Zhou et al., 2014) and AML state.

oncoprotein will both abrogate tumor progression in Ewing Sarcoma (Seong et al., 2021). This principle may also be applicable in the case of IRF8 and PU.1 in leukemia, as well as other cancer dependencies, and further work is warranted to fully test these possibilities.

TFs are able to specifically modulate refined transcriptional programs and are sufficient to direct cell type specification, including differentiation, dedifferentiation and *trans*-differentiation (Fong and Tapscott, 2013; Henley and Koehler, 2021; Lambert et al., 2018; Takahashi and Yamanaka, 2016). It has been proposed that a TF inhibitor would theoretically confer high potency and specificity, in comparison to a signaling factor inhibitor that may impair multiple signaling pathways leading to unwanted toxicities (Bhagwat and Vakoc, 2015; Henley and Koehler, 2021). Despite obstacles in developing TF specific inhibitors (Bushweller, 2019; Darnell, 2002) and no MEF2D/IRF8 inhibitor available, advances have been made via different strategies, including protein-protein interface disruption and PROTAC/molecular glue-based degradation (Henley and Koehler, 2021), and targeting the druggable upstream regulators of the TFs (such as DOT1L, BRD4, ZMYND8 and SIK3) as an actionable strategy (Bernt et al., 2011; Cao et al., 2021; Daigle et al., 2011; Tarumoto et al., 2020; Zuber et al., 2011b). Because mouse models of Mef2d knockout showed neither apparent developmental abnormalities (Kim et al., 2008; Pon and Marra, 2015) nor defects in T, B cell or myeloid cell development (Pattison et al., 2020), we predict that therapeutic inhibition of MEF2D function or pathways may be an attractive future direction for selectively targeting AML with minimal toxicity.

Limitations of study

Although our analysis and *in vitro* data showed MEF2D is an AML-selective dependency, further work is needed *in vivo* to fully determine the role of MEF2D in leukemia progression as well as normal hematopoiesis. Our data suggest MEF2D and IRF8 may also function independently to sustain AML, but the

underlying mechanism remains to be elucidated. MEF2D-IRF8 circuit can be activated through KMT2A rearrangement; however, we did not evaluate whether this circuit is required for leukemia initiation, and whether this circuit can be self-maintained or requires additional factors after activation. Another limitation of our study is that we did not evaluate the requirement of MEF2D in a more clinically relevant model, such as patient derived xenograft (PDX) or primary patient cells because of the challenge in conducting genome editing in these cells and lack of small molecule inhibitor against this circuit.

STAR★METHODS

Detailed methods are provided in the online version of this paper and include the following:

- KEY RESOURCES TABLE
- RESOURCE AVAILABILITY
  - Lead contact
  - Materials availability
  - Data and code availability
- EXPERIMENTAL MODEL AND SUBJECT DETAILS
  - Cell lines
  - Primary AML samples
  - Mouse models
- METHOD DETAILS
  - sgRNA and plasmid cloning
  - Virus production and transduction
  - Competition-based cell proliferation assay
  - Immunoblotting
  - Colony formation assay
  - RNA-seq
  - ChIP-sequencing and ChIP-qPCR
  - CUT&RUN and CUT&RUN qPCR
  - RT-PCR
  - Deletion of regulatory elements
  - Identification of leukemia-selective TF dependencies
  - RNA-seq analysis
  - ChIP-seq and CUT&RUN processing
  - Peak overlap and shifting analysis
  - Peak overlap and differential analysis
- QUANTIFICATION AND STATISTICAL ANALYSIS

SUPPLEMENTAL INFORMATION

Supplemental information can be found online at https://doi.org/10.1016/j.isci.2022.105139.

ACKNOWLEDGMENTS

We thank James D. Griffin for OCI-AML5 cell line, James C. Mulloy for retroviral human leukemia lines, Will Bailis for sharing Cas9+ murine BM cells, Mitchell J. Weiss and Ruopeng Feng for helpful suggestions, Yeqiao Zhou and Robert B. Faryabi for enhancer analysis, and Krista A. Budinich for helping with the sgRNA cloning and immunoblotting. This work was supported by NIH grant R01 CA258904 (to J.S.) and NIH training grant T32 DK07780 (to B.P.)

AUTHOR CONTRIBUTIONS

Z.C. and J.S. conceived of and designed the study. B.Y.P. and Z.C. performed most experiments and analyzed data; F.A. contributed to the murine colony formation assay; Q.C. established the Cas12a-mediated deletion system; Z.Z. contributed to the CUT&RUN experiments. H.H and Z.C. analyzed and interpreted the NGS data. J.Q. provided the dTAG-47 compound. K.M.B, S.L.B., Z.C., and J.S. supervised the research. B.Y.P., Z.C., and J.S. wrote the manuscript with inputs from all authors.

DECLARATION OF INTERESTS

The authors declare no conflict of interest.

Received: October 25, 2021
Revised: August 5, 2022
Accepted: September 10, 2022
Published: October 21, 2022

REFERENCES

Anders, S., Pyl, P.T., and Huber, W. (2015). HTSeq–a Python framework to work with high-throughput sequencing data. Bioinformatics *31*, 166–169. https://doi.org/10.1093/bioinformatics/btu638.

Antony-Debré, I., Paul, A., Leite, J., Mitchell, K., Kim, H.M., Carvajal, L.A., Todorova, T.I., Huang, K., Kumar, A., Farahat, A.A., et al. (2017). Pharmacological inhibition of the transcription factor PU.1 in leukemia. J. Clin. Invest. *127*, 4297–4313. https://doi.org/10.1172/JCI92504.

Assi, S.A., Imperato, M.R., Coleman, D.J.L., Pickin, A., Potluri, S., Ptasinska, A., Chin, P.S., Blair, H., Cauchy, P., James, S.R., et al. (2019). Subtype-specific regulatory network rewiring in acute myeloid leukemia. Nat. Genet. *51*, 151–162. https://doi.org/10.1038/s41588-018-0270-1.

Bahr, C., von Paleske, L., Uslu, V.V., Remeseiro, S., Takayama, N., Ng, S.W., Murison, A., Langenfeld, K., Petretich, M., Scognamiglio, R., et al. (2018). A Myc enhancer cluster regulates normal and leukaemic haematopoietic stem cell hierarchies. Nature *553*, 515–520. https://doi.org/10.1038/nature25193.

Barabé, F., Gil, L., Celton, M., Bergeron, A., Lamontagne, V., Roques, É., Lagacé, K., Forest, A., Johnson, R., Pécheux, L., et al. (2017). Modeling human MLL-AF9 translocated acute myeloid leukemia from single donors reveals RET as a potential therapeutic target. Leukemia *31*, 1166–1176. https://doi.org/10.1038/leu.2016.302.

Barretina, J., Caponigro, G., Stransky, N., Venkatesan, K., Margolin, A.A., Kim, S., Wilson, C.J., Lehár, J., Kryukov, G.V., Sonkin, D., et al. (2012). The Cancer Cell Line Encyclopedia enables predictive modelling of anticancer drug sensitivity. Nature *483*, 603–607. https://doi.org/10.1038/nature11003.

Bernt, K.M., Zhu, N., Sinha, A.U., Vempati, S., Faber, J., Krivtsov, A.V., Feng, Z., Punt, N., Daigle, A., Bullinger, L., et al. (2011). MLL-Rearranged leukemia is dependent on aberrant H3K79 methylation by DOT1L. Cancer Cell *20*, 66–78. https://doi.org/10.1016/j.ccr.2011.06.010.

Bhagwat, A.S., and Vakoc, C.R. (2015). Targeting transcription factors in cancer. Trends Cancer *1*, 53–65. https://doi.org/10.1016/j.trecan.2015.07.001.

Boyer, L.A., Lee, T.I., Cole, M.F., Johnstone, S.E., Levine, S.S., Zucker, J.P., Guenther, M.G., Kumar, R.M., Murray, H.L., Jenner, R.G., et al. (2005). Core transcriptional regulatory circuitry in human embryonic stem cells. Cell *122*, 947–956. https://doi.org/10.1016/j.cell.2005.08.020.

Bradner, J.E., Hnisz, D., and Young, R.A. (2017). Transcriptional addiction in cancer. Cell *168*, 629–643. https://doi.org/10.1016/j.cell.2016.12.013.

Buganim, Y., Faddah, D.A., and Jaenisch, R. (2013). Mechanisms and models of somatic cell reprogramming. Nat. Rev. Genet. *14*, 427–439. https://doi.org/10.1038/nrg3473.

Bushweller, J.H. (2019). Targeting transcription factors in cancer - from undruggable to reality. Nat. Rev. Cancer *19*, 611–624. https://doi.org/10.1038/s41568-019-0196-7.

Cancer Genome Atlas Research Network, Ley, T.J., Miller, C., Ding, L., Raphael, B.J., Mungall, A.J., Robertson, A.G., Hoadley, K., Triche, T.J., Laird, P.W., et al. (2013). Genomic and epigenomic landscapes of adult de novo acute myeloid leukemia. N. Engl. J. Med. *368*, 2059–2074. https://doi.org/10.1056/NEJMoa1301689.

Cao, Z., Budinich, K.A., Huang, H., Ren, D., Lu, B., Zhang, Z., Chen, Q., Zhou, Y., Huang, Y.-H., Alikarami, F., et al. (2021). ZMYND8-regulated IRF8 transcription axis is an acute myeloid leukemia dependency. Mol. Cell *81*, 3604–3622.e10. https://doi.org/10.1016/j.molcel.2021.07.018.

Chen, Z., Arai, E., Khan, O., Zhang, Z., Ngiow, S.F., He, Y., Huang, H., Manne, S., Cao, Z., Baxter, A.E., et al. (2021). In vivo CD8+ T cell CRISPR screening reveals control by Fli1 in infection and cancer. Cell *184*, 1262–1280.e22. https://doi.org/10.1016/j.cell.2021.02.019.

Corces, M.R., Buenrostro, J.D., Wu, B., Greenside, P.G., Chan, S.M., Koenig, J.L., Snyder, M.P., Pritchard, J.K., Kundaje, A., Greenleaf, W.J., et al. (2016). Lineage-specific and single-cell chromatin accessibility charts human hematopoiesis and leukemia evolution. Nat. Genet. *48*, 1193–1203. https://doi.org/10.1038/ng.3646.

Daigle, S.R., Olhava, E.J., Therkelsen, C.A., Majer, C.R., Sneeringer, C.J., Song, J., Johnston, L.D., Scott, M.P., Smith, J.J., Xiao, Y., et al. (2011). Selective killing of mixed lineage leukemia cells by a potent small-molecule DOT1L inhibitor. Cancer Cell *20*, 53–65. https://doi.org/10.1016/j.ccr.2011.06.009.

Darnell, J.E. (2002). Transcription factors as targets for cancer therapy. Nat. Rev. Cancer *2*, 740–749. https://doi.org/10.1038/nrc906.

Davis, R.L., Weintraub, H., and Lassar, A.B. (1987). Expression of a single transfected cDNA converts fibroblasts to myoblasts. Cell *51*, 987–1000. https://doi.org/10.1016/0092-8674(87)90585-x.

Dempster, J.M., Rossen, J., Kazachkova, M., Pan, J., Kugener, G., Root, D.E., and Tsherniak, A. (2019). Extracting biological insights from the project achilles genome-scale CRISPR screens in cancer cell lines. Preprint at bioRxiv. https://doi.org/10.1101/720243.

Dharia, N.V., Kugener, G., Guenther, L.M., Malone, C.F., Durbin, A.D., Hong, A.L., Howard, T.P., Bandopadhayay, P., Wechsler, C.S., Fung, I., et al. (2021). A first-generation pediatric cancer dependency map. Nat. Genet. *53*, 529–538. https://doi.org/10.1038/s41588-021-00819-w.

Di Giorgio, E., Hancock, W.W., and Brancolini, C. (2018). MEF2 and the tumorigenic process, hic sunt leones. Biochim. Biophys. Acta. Rev. Cancer *1870*, 261–273. https://doi.org/10.1016/j.bbcan.2018.05.007.

Dobin, A., Davis, C.A., Schlesinger, F., Drenkow, J., Zaleski, C., Jha, S., Batut, P., Chaisson, M., and Gingeras, T.R. (2013). STAR: ultrafast universal RNA-seq aligner. Bioinformatics *29*, 15–21. https://doi.org/10.1093/bioinformatics/bts635.

Doench, J.G., Fusi, N., Sullender, M., Hegde, M., Vaimberg, E.W., Donovan, K.F., Smith, I., Tothova, Z., Wilen, C., Orchard, R., et al. (2016). Optimized sgRNA design to maximize activity and minimize off-target effects of CRISPR-Cas9. Nat. Biotechnol. *34*, 184–191. https://doi.org/10.1038/nbt.3437.

Döhner, H., Weisdorf, D.J., and Bloomfield, C.D. (2015). Acute myeloid leukemia. N. Engl. J. Med. *373*, 1136–1152. https://doi.org/10.1056/NEJMra1406184.

Eisenbeis, C.F., Singh, H., and Storb, U. (1995). Pip, a novel IRF family member, is a lymphoid-specific, PU.1-dependent transcriptional activator. Genes Dev. *9*, 1377–1387. https://doi.org/10.1101/gad.9.11.1377.

Escalante, C.R., Brass, A.L., Pongubala, J.M.R., Shatova, E., Shen, L., Singh, H., and Aggarwal, A.K. (2002). Crystal structure of PU.1/IRF-4/DNA ternary complex. Mol. Cell *10*, 1097–1105. https://doi.org/10.1016/S1097-2765(02)00703-7.

Fong, A.P., and Tapscott, S.J. (2013). Skeletal muscle programming and re-programming. Curr. Opin. Genet. Dev. *23*, 568–573. https://doi.org/10.1016/j.gde.2013.05.002.

Fulco, C.P., Munschauer, M., Anyoha, R., Munson, G., Grossman, S.R., Perez, E.M., Kane, M., Cleary, B., Lander, E.S., and Engreitz, J.M. (2016). Systematic mapping of functional enhancer-promoter connections with CRISPR interference. Science *354*, 769–773. https://doi.org/10.1126/science.aag2445.

Gaillard, C., Surianarayanan, S., Bentley, T., Warr, M.R., Fitch, B., Geng, H., Passegué, E., de Thé, H., and Kogan, S.C. (2018). Identification of IRF8 as a potent tumor suppressor in murine acute promyelocytic leukemia. Blood Adv. *2*, 2462–2466. https://doi.org/10.1182/bloodadvances.2018018929.

Gier, R.A., Budinich, K.A., Evitt, N.H., Cao, Z., Freilich, E.S., Chen, Q., Qi, J., Lan, Y., Kohli, R.M., and Shi, J. (2020). High-performance CRISPR-Cas12a genome editing for combinatorial genetic screening. Nat. Commun. *11*, 3455. https://doi.org/10.1038/s41467-020-17209-1.

Gilbert, L.A., Larson, M.H., Morsut, L., Liu, Z., Brar, G.A., Torres, S.E., Stern-Ginossar, N., Brandman, O., Whitehead, E.H., Doudna, J.A., et al. (2013).

CRISPR-mediated modular RNA-guided regulation of transcription in eukaryotes. Cell *154*, 442–451. https://doi.org/10.1016/j.cell.2013.06.044.

Gozdecka, M., Meduri, E., Mazan, M., Tzelepis, K., Dudek, M., Knights, A.J., Pardo, M., Yu, L., Choudhary, J.S., Metzakopian, E., et al. (2018). UTX-mediated enhancer and chromatin remodeling suppresses myeloid leukemogenesis through noncatalytic inverse regulation of ETS and GATA programs. Nat. Genet. *50*, 883–894. https://doi.org/10.1038/s41588-018-0114-z.

Graf, T., and Enver, T. (2009). Forcing cells to change lineages. Nature *462*, 587–594. https://doi.org/10.1038/nature08533.

Gröbner, S.N., Worst, B.C., Weischenfeldt, J., Buchhalter, I., Kleinheinz, K., Rudneva, V.A., Johann, P.D., Balasubramanian, G.P., Segura-Wang, M., Brabetz, S., et al. (2018). The landscape of genomic alterations across childhood cancers. Nature *555*, 321–327. https://doi.org/10.1038/nature25480.

Gu, X., Ebrahem, Q., Mahfouz, R.Z., Hasipek, M., Enane, F., Radivoyevitch, T., Rapin, N., Przychodzen, B., Hu, Z., Balusu, R., et al. (2018). Leukemogenic nucleophosmin mutation disrupts the transcription factor hub that regulates granulomonocytic fates. J. Clin. Invest. *128*, 4260–4279. https://doi.org/10.1172/JCI97117.

Gu, Z., Churchman, M., Roberts, K., Li, Y., Liu, Y., Harvey, R.C., McCastlain, K., Reshmi, S.C., Payne-Turner, D., Iacobucci, I., et al. (2016a). Genomic analyses identify recurrent MEF2D fusions in acute lymphoblastic leukaemia. Nat. Commun. *7*, 13331. https://doi.org/10.1038/ncomms13331.

Gu, Z., Eils, R., and Schlesner, M. (2016b). Complex heatmaps reveal patterns and correlations in multidimensional genomic data. Bioinformatics *32*, 2847–2849. https://doi.org/10.1093/bioinformatics/btw313.

Ha, V.L., Luong, A., Li, F., Casero, D., Malvar, J., Kim, Y.M., Bhatia, R., Crooks, G.M., and Parekh, C. (2017). The T-ALL related gene BCL11B regulates the initial stages of human T-cell differentiation. Leukemia *31*, 2503–2514. https://doi.org/10.1038/leu.2017.70.

Harada, T., Heshmati, Y., Kalfon, J., Perez, M.W., Xavier Ferrucio, J., Ewers, J., Hubbell Engler, B., Kossenkov, A., Ellegast, J.M., Yi, J.S., et al. (2022). A distinct core regulatory module enforces oncogene expression in KMT2A-rearranged leukemia. Genes Dev. *36*, 368–389. https://doi.org/10.1101/gad.349284.121.

Heinz, S., Benner, C., Spann, N., Bertolino, E., Lin, Y.C., Laslo, P., Cheng, J.X., Murre, C., Singh, H., and Glass, C.K. (2010). Simple combinations of lineage-determining transcription factors prime cis-regulatory elements required for macrophage and B cell identities. Mol. Cell *38*, 576–589. https://doi.org/10.1016/j.molcel.2010.05.004.

Henley, M.J., and Koehler, A.N. (2021). Advances in targeting 'undruggable' transcription factors with small molecules. Nat. Rev. Drug Discov. *20*, 669–688. https://doi.org/10.1038/s41573-021-00199-0.

Holtschke, T., Löhler, J., Kanno, Y., Fehr, T., Giese, N., Rosenbauer, F., Lou, J., Knobeloch, K.-P., Gabriele, L., Waring, J.F., et al. (1996). Immunodeficiency and chronic myelogenous leukemia-like syndrome in mice with a targeted mutation of the ICSBP gene. Cell *87*, 307–317. https://doi.org/10.1016/S0092-8674(00)81348-3.

Horton, S.J., Jaques, J., Woolthuis, C., van Dijk, J., Mesuraca, M., Huls, G., Morrone, G., Vellenga, E., and Schuringa, J.J. (2013). MLL-AF9-mediated immortalization of human hematopoietic cells along different lineages changes during ontogeny. Leukemia *27*, 1116–1126. https://doi.org/10.1038/leu.2012.343.

Jourquin, J., Duncan, D., Shi, Z., and Zhang, B. (2012). GLAD4U: deriving and prioritizing gene lists from PubMed literature. BMC Genom. *13* (*Suppl 8*), S20. https://doi.org/10.1186/1471-2164-13-S8-S20.

Khwaja, A., Bjorkholm, M., Gale, R.E., Levine, R.L., Jordan, C.T., Ehninger, G., Bloomfield, C.D., Estey, E., Burnett, A., Cornelissen, J.J., et al. (2016). Acute myeloid leukaemia. Nat. Rev. Dis. Primers *2*, 16010. https://doi.org/10.1038/nrdp.2016.10.

Kim, Y., Phan, D., van Rooij, E., Wang, D.-Z., McAnally, J., Qi, X., Richardson, J.A., Hill, J.A., Bassel-Duby, R., and Olson, E.N. (2008). The MEF2D transcription factor mediates stress-dependent cardiac remodeling in mice. J. Clin. Invest. *118*, 124–132. https://doi.org/10.1172/JCI33255.

Kollmann, S., Grundschober, E., Maurer, B., Warsch, W., Grausenburger, R., Edlinger, L., Huuhtanen, J., Lagger, S., Hennighausen, L., Valent, P., et al. (2019). Twins with different personalities: STAT5B—but not STAT5A—has a key role in BCR/ABL-induced leukemia. Leukemia *33*, 1583–1597. https://doi.org/10.1038/s41375-018-0369-5.

Krivtsov, A.V., Twomey, D., Feng, Z., Stubbs, M.C., Wang, Y., Faber, J., Levine, J.E., Wang, J., Hahn, W.C., Gilliland, D.G., et al. (2006). Transformation from committed progenitor to leukaemia stem cell initiated by MLL–AF9. Nature *442*, 818–822. https://doi.org/10.1038/nature04980.

Krivtsov, A.V., Evans, K., Gadrey, J.Y., Eschle, B.K., Hatton, C., Uckelmann, H.J., Ross, K.N., Perner, F., Olsen, S.N., Pritchard, T., et al. (2019). A menin-MLL inhibitor induces specific chromatin changes and eradicates disease in models of MLL-rearranged leukemia. Cancer Cell *36*, 660–673.e11. https://doi.org/10.1016/j.ccell.2019.11.001.

Kurotaki, D., Nakabayashi, J., Nishiyama, A., Sasaki, H., Kawase, W., Kaneko, N., Ochiai, K., Igarashi, K., Ozato, K., Suzuki, Y., and Tamura, T. (2018). Transcription factor IRF8 governs enhancer landscape dynamics in mononuclear phagocyte progenitors. Cell Rep. *22*, 2628–2641. https://doi.org/10.1016/j.celrep.2018.02.048.

Lambert, S.A., Jolma, A., Campitelli, L.F., Das, P.K., Yin, Y., Albu, M., Chen, X., Taipale, J., Hughes, T.R., and Weirauch, M.T. (2018). The human transcription factors. Cell *172*, 650–665. https://doi.org/10.1016/j.cell.2018.01.029.

Langmead, B., and Salzberg, S.L. (2012). Fast gapped-read alignment with Bowtie 2. Nat. Methods *9*, 357–359. https://doi.org/10.1038/nmeth.1923.

Lee, T.I., and Young, R.A. (2013). Transcriptional regulation and its misregulation in disease. Cell *152*, 1237–1251. https://doi.org/10.1016/j.cell.2013.02.014.

Li, H., Handsaker, B., Wysoker, A., Fennell, T., Ruan, J., Homer, N., Marth, G., Abecasis, G., and Durbin, R.; 1000 Genome Project Data Processing Subgroup (2009). The sequence alignment/map format and SAMtools. Bioinformatics *25*, 2078–2079. https://doi.org/10.1093/bioinformatics/btp352.

Li, H., Mar, B.G., Zhang, H., Puram, R.V., Vazquez, F., Weir, B.A., Hahn, W.C., Ebert, B., and Pellman, D. (2017). The EMT regulator ZEB2 is a novel dependency of human and murine acute myeloid leukemia. Blood *129*, 497–508. https://doi.org/10.1182/blood-2016-05-714493.

Li, S., Mason, C.E., and Melnick, A. (2016). Genetic and epigenetic heterogeneity in acute myeloid leukemia. Curr. Opin. Genet. Dev. *36*, 100–106. https://doi.org/10.1016/j.gde.2016.03.011.

Liao, Y., Wang, J., Jaehnig, E.J., Shi, Z., and Zhang, B. (2019). WebGestalt 2019: gene set analysis toolkit with revamped UIs and APIs. Nucleic Acids Res. *47*, W199–W205. https://doi.org/10.1093/nar/gkz401.

Liberzon, A., Birger, C., Thorvaldsdóttir, H., Ghandi, M., Mesirov, J., and Tamayo, P. (2015). The molecular signatures Database hallmark gene set collection. Cell Syst. *1*, 417–425. https://doi.org/10.1016/j.cels.2015.12.004.

Liss, F., Frech, M., Wang, Y., Giel, G., Fischer, S., Simon, C., Weber, L.M., Nist, A., Stiewe, T., Neubauer, A., et al. (2021). IRF8 is an AML-specific susceptibility factor that regulates signaling pathways and proliferation of AML cells. Cancers *13*, 764. https://doi.org/10.3390/cancers13040764.

Liu, N., Williams, A.H., Kim, Y., McAnally, J., Bezprozvannaya, S., Sutherland, L.B., Richardson, J.A., Bassel-Duby, R., and Olson, E.N. (2007). An intragenic MEF2-dependent enhancer directs muscle-specific expression of microRNAs 1 and 133. Proc. Natl. Acad. Sci. USA *104*, 20844–20849. https://doi.org/10.1073/pnas.0710558105.

Liu, N., Hargreaves, V.V., Zhu, Q., Kurland, J.V., Hong, J., Kim, W., Sher, F., Macias-Trevino, C., Rogers, J.M., Kurita, R., et al. (2018). Direct promoter repression by BCL11A controls the fetal to adult hemoglobin switch. Cell *173*, 430–442.e17. https://doi.org/10.1016/j.cell.2018.03.016.

Liu, Y.-F., Wang, B.-Y., Zhang, W.-N., Huang, J.-Y., Li, B.-S., Zhang, M., Jiang, L., Li, J.-F., Wang, M.-J., Dai, Y.-J., et al. (2016). Genomic profiling of adult and pediatric B-cell acute lymphoblastic leukemia. EBioMedicine *8*, 173–183. https://doi.org/10.1016/j.ebiom.2016.04.038.

Love, M.I., Huber, W., and Anders, S. (2014). Moderated estimation of fold change and dispersion for RNA-seq data with DESeq2. Genome Biol. *15*, 550. https://doi.org/10.1186/s13059-014-0550-8.

Lu, B., Klingbeil, O., Tarumoto, Y., Somerville, T.D.D., Huang, Y.-H., Wei, Y., Wai, D.C., Low, J.K.K., Milazzo, J.P., Wu, X.S., et al. (2018). A transcription factor addiction in leukemia imposed by the MLL promoter sequence. Cancer

Cell *34*, 970–981.e8. https://doi.org/10.1016/j.ccell.2018.10.015.

Lu, R., Medina, K.L., Lancki, D.W., and Singh, H. (2003). IRF-4, 8 orchestrate the pre-B-to-B transition in lymphocyte development. Genes Dev. *17*, 1703–1708. https://doi.org/10.1101/gad.1104803.

Ma, L., Liu, J., Liu, L., Duan, G., Wang, Q., Xu, Y., Xia, F., Shan, J., Shen, J., Yang, Z., et al. (2014). Overexpression of the transcription factor MEF2D in hepatocellular carcinoma sustains malignant character by suppressing G2-M transition genes. Cancer Res. *74*, 1452–1462. https://doi.org/10.1158/0008-5472.CAN-13-2171.

Ma, X., Liu, Y., Liu, Y., Alexandrov, L.B., Edmonson, M.N., Gawad, C., Zhou, X., Li, Y., Rusch, M.C., Easton, J., et al. (2018). Pan-cancer genome and transcriptome analyses of 1, 699 paediatric leukaemias and solid tumours. Nature *555*, 371–376. https://doi.org/10.1038/nature25795.

Martinez-Soria, N., McKenzie, L., Draper, J., Ptasinska, A., Issa, H., Potluri, S., Blair, H.J., Pickin, A., Isa, A., Chin, P.S., et al. (2018). The oncogenic transcription factor RUNX1/ETO corrupts cell cycle regulation to drive leukemic transformation. Cancer Cell *34*, 626–642.e8. https://doi.org/10.1016/j.ccell.2018.08.015.

McKenzie, M.D., Ghisi, M., Oxley, E.P., Ngo, S., Cimmino, L., Esnault, C., Liu, R., Salmon, J.M., Bell, C.C., Ahmed, N., et al. (2019). Interconversion between tumorigenic and differentiated states in acute myeloid leukemia. Cell Stem Cell *25*, 258–272.e9. https://doi.org/10.1016/j.stem.2019.07.001.

Meyers, R.M., Bryan, J.G., McFarland, J.M., Weir, B.A., Sizemore, A.E., Xu, H., Dharia, N.V., Montgomery, P.G., Cowley, G.S., Pantel, S., et al. (2017). Computational correction of copy-number effect improves specificity of CRISPR-Cas9 essentiality screens in cancer cells. Nat. Genet. *49*, 1779–1784. https://doi.org/10.1038/ng.3984.

Minderjahn, J., Schmidt, A., Fuchs, A., Schill, R., Raithel, J., Babina, M., Schmidl, C., Gebhard, C., Schmidhofer, S., Mendes, K., et al. (2020). Mechanisms governing the pioneering and redistribution capabilities of the non-classical pioneer PU.1. Nat. Commun. *11*, 402. https://doi.org/10.1038/s41467-019-13960-2.

Mohaghegh, N., Bray, D., Keenan, J., Penvose, A., Andrilenas, K.K., Ramlall, V., and Siggers, T. (2019). NextPBM: a platform to study cell-specific transcription factor binding and cooperativity. Nucleic Acids Res. *47*, e31. https://doi.org/10.1093/nar/gkz020.

Murakami, K., Sasaki, H., Nishiyama, A., Kurotaki, D., Kawase, W., Ban, T., Nakabayashi, J., Kanzaki, S., Sekita, Y., Nakajima, H., et al. (2021). A RUNX–CBFβ-driven enhancer directs the Irf8 dose-dependent lineage choice between DCs and monocytes. Nat. Immunol. *22*, 301–311. https://doi.org/10.1038/s41590-021-00871-y.

Nabet, B., Roberts, J.M., Buckley, D.L., Paulk, J., Dastjerdi, S., Yang, A., Leggett, A.L., Erb, M.A., Lawlor, M.A., Souza, A., et al. (2018). The dTAG system for immediate and target-specific protein degradation. Nat. Chem. Biol. *14*, 431–441. https://doi.org/10.1038/s41589-018-0021-8.

Ohki, K., Kiyokawa, N., Saito, Y., Hirabayashi, S., Nakabayashi, K., Ichikawa, H., Momozawa, Y., Okamura, K., Yoshimi, A., Ogata-Kawata, H., et al. (2019). Clinical and molecular characteristics of MEF2D fusion-positive B-cell precursor acute lymphoblastic leukemia in childhood, including a novel translocation resulting in MEF2D-HNRNPH1 gene fusion. Haematologica *104*, 128–137. https://doi.org/10.3324/haematol.2017.186320.

Ohlsson, E., Hasemann, M.S., Willer, A., Lauridsen, F.K.B., Rapin, N., Jendholm, J., and Porse, B.T. (2014). Initiation of MLL-rearranged AML is dependent on C/EBPα. J. Exp. Med. *211*, 5–13. https://doi.org/10.1084/jem.20130932.

Pang, S.H.M., Minnich, M., Gangatirkar, P., Zheng, Z., Ebert, A., Song, G., Dickins, R.A., Corcoran, L.M., Mullighan, C.G., Busslinger, M., et al. (2016). PU.1 cooperates with IRF4 and IRF8 to suppress pre-B-cell leukemia. Leukemia *30*, 1375–1387. https://doi.org/10.1038/leu.2016.27.

Pattison, M.J., Naik, R.J., Reyskens, K.M.S.E., and Arthur, J.S.C. (2020). Loss of Mef2D function enhances TLR induced IL-10 production in macrophages. Biosci. Rep. *40*. BSR20201859. https://doi.org/10.1042/BSR20201859.

Pon, J.R., and Marra, M.A. (2016). MEF2 transcription factors: developmental regulators and emerging cancer genes. Oncotarget *7*, 2297–2312. https://doi.org/10.18632/oncotarget.6223.

Poppe, M., Wittig, S., Jurida, L., Bartkuhn, M., Wilhelm, J., Müller, H., Beuerlein, K., Karl, N., Bhuju, S., Ziebuhr, J., et al. (2017). The NF-κB-dependent and -independent transcriptome and chromatin landscapes of human coronavirus 229E-infected cells. PLoS Pathog. *13*, e1006286. https://doi.org/10.1371/journal.ppat.1006286.

Potthoff, M.J., and Olson, E.N. (2007). MEF2: a central regulator of diverse developmental programs. Development *134*, 4131–4140. https://doi.org/10.1242/dev.008367.

Quinlan, A.R., and Hall, I.M. (2010). BEDTools: a flexible suite of utilities for comparing genomic features. Bioinformatics *26*, 841–842. https://doi.org/10.1093/bioinformatics/btq033.

Ramírez, F., Ryan, D.P., Grüning, B., Bhardwaj, V., Kilpert, F., Richter, A.S., Heyne, S., Dündar, F., and Manke, T. (2016). deepTools2: a next generation web server for deep-sequencing data analysis. Nucleic Acids Res. *44*, W160–W165. https://doi.org/10.1093/nar/gkw257.

Rathert, P., Roth, M., Neumann, T., Muerdter, F., Roe, J.-S., Muhar, M., Deswal, S., Cerny-Reiterer, S., Peter, B., Jude, J., et al. (2015). Transcriptional plasticity promotes primary and acquired resistance to BET inhibition. Nature *525*, 543–547. https://doi.org/10.1038/nature14898.

Roe, J.-S., Mercan, F., Rivera, K., Pappin, D.J., and Vakoc, C.R. (2015). BET bromodomain inhibition suppresses the function of hematopoietic transcription factors in acute myeloid leukemia. Mol. Cell *58*, 1028–1039. https://doi.org/10.1016/j.molcel.2015.04.011.

Rosenbauer, F., Koschmieder, S., Steidl, U., and Tenen, D.G. (2005). Effect of transcription-factor concentrations on leukemic stem cells. Blood *106*, 1519–1524. https://doi.org/10.1182/blood-2005-02-0717.

Saito, Y., Kitamura, H., Hijikata, A., Tomizawa-Murasawa, M., Tanaka, S., Takagi, S., Uchida, N., Suzuki, N., Sone, A., Najima, Y., et al. (2010). Identification of therapeutic targets for quiescent, chemotherapy-resistant human leukemia stem cells. Sci. Transl. Med. *2*, 17ra9. https://doi.org/10.1126/scitranslmed.3000349.

Secker, K.-A., Bruns, L., Keppeler, H., Jeong, J., Hentrich, T., Schulze-Hentrich, J.M., Mankel, B., Fend, F., Schneidawind, D., and Schneidawind, C. (2020). Only hematopoietic stem and progenitor cells from cord blood are susceptible to malignant transformation by MLL-AF4 translocations. Cancers *12*, E1487. https://doi.org/10.3390/cancers12061487.

Seong, B.K.A., Dharia, N.V., Lin, S., Donovan, K.A., Chong, S., Robichaud, A., Conway, A., Hamze, A., Ross, L., Alexe, G., et al. (2021). TRIM8 modulates the EWS/FLI oncoprotein to promote survival in Ewing sarcoma. Cancer Cell *39*, 1262–1278.e7. https://doi.org/10.1016/j.ccell.2021.07.003.

Shi, J., Whyte, W.A., Zepeda-Mendoza, C.J., Milazzo, J.P., Shen, C., Roe, J.-S., Minder, J.L., Mercan, F., Wang, E., Eckersley-Maslin, M.A., et al. (2013). Role of SWI/SNF in acute leukemia maintenance and enhancer-mediated Myc regulation. Genes Dev. *27*, 2648–2662. https://doi.org/10.1101/gad.232710.113.

Shimizu, R., Engel, J.D., and Yamamoto, M. (2008). GATA1-related leukaemias. Nat. Rev. Cancer *8*, 279–287. https://doi.org/10.1038/nrc2348.

Shyamsunder, P., Shanmugasundaram, M., Mayakonda, A., Dakle, P., Teoh, W.W., Han, L., Kanojia, D., Lim, M.C., Fullwood, M., An, O., et al. (2019). Identification of a novel enhancer of CEBPE essential for granulocytic differentiation. Blood *133*, 2507–2517. https://doi.org/10.1182/blood.2018886077.

Skene, P.J., Henikoff, J.G., and Henikoff, S. (2018). Targeted in situ genome-wide profiling with high efficiency for low cell numbers. Nat. Protoc. *13*, 1006–1019. https://doi.org/10.1038/nprot.2018.015.

Staal, F.J.T., Famili, F., Garcia Perez, L., and Pike-Overzet, K. (2016). Aberrant Wnt signaling in leukemia. Cancers *8*, 78. https://doi.org/10.3390/cancers8090078.

Suzuki, K., Okuno, Y., Kawashima, N., Muramatsu, H., Okuno, T., Wang, X., Kataoka, S., Sekiya, Y., Hamada, M., Murakami, N., et al. (2016). MEF2D-BCL9 fusion gene is associated with high-risk acute B-cell precursor lymphoblastic leukemia in adolescents. J. Clin. Oncol. *34*, 3451–3459. https://doi.org/10.1200/JCO.2016.66.5547.

Takahashi, K., and Yamanaka, S. (2016). A decade of transcription factor-mediated reprogramming to pluripotency. Nat. Rev. Mol. Cell Biol. *17*, 183–193. https://doi.org/10.1038/nrm.2016.8.

Tamura, T., Kurotaki, D., and Koizumi, S.i. (2015). Regulation of myelopoiesis by the transcription factor IRF8. Int. J. Hematol. *101*, 342–351. https://doi.org/10.1007/s12185-015-1761-9.

Tang, Y.Y., Shi, J., Zhang, L., Davis, A., Bravo, J., Warren, A.J., Speck, N.A., and Bushweller, J.H. (2000). Energetic and functional contribution of residues in the core binding factor beta (CBFbeta) subunit to heterodimerization with CBFalpha. J. Biol. Chem. *275*, 39579–39588. https://doi.org/10.1074/jbc.M007350200.

Tarumoto, Y., Lu, B., Somerville, T.D.D., Huang, Y.-H., Milazzo, J.P., Wu, X.S., Klingbeil, O., El Demerdash, O., Shi, J., and Vakoc, C.R. (2018). LKB1, Salt-Inducible Kinases, and MEF2C are linked dependencies in acute myeloid leukemia. Mol. Cell *69*, 1017–1027.e6. https://doi.org/10.1016/j.molcel.2018.02.011.

Tarumoto, Y., Lin, S., Wang, J., Milazzo, J.P., Xu, Y., Lu, B., Yang, Z., Wei, Y., Polyanskaya, S., Wunderlich, M., et al. (2020). Salt-inducible kinase inhibition suppresses acute myeloid leukemia progression in vivo. Blood *135*, 56–70. https://doi.org/10.1182/blood.2019001576.

Trapnell, C., Hendrickson, D.G., Sauvageau, M., Goff, L., Rinn, J.L., and Pachter, L. (2013). Differential analysis of gene regulation at transcript resolution with RNA-seq. Nat. Biotechnol. *31*, 46–53. https://doi.org/10.1038/nbt.2450.

Tsherniak, A., Vazquez, F., Montgomery, P.G., Weir, B.A., Kryukov, G., Cowley, G.S., Gill, S., Harrington, W.F., Pantel, S., Krill-Burger, J.M., et al. (2017). Defining a cancer dependency map. Cell *170*, 564–576.e16. https://doi.org/10.1016/j.cell.2017.06.010.

Tsuzuki, S., Yasuda, T., Kojima, S., Kawazu, M., Akahane, K., Inukai, T., Imaizumi, M., Morishita, T., Miyamura, K., Ueno, T., et al. (2020). Targeting MEF2D-fusion oncogenic transcriptional circuitries in B-cell precursor acute lymphoblastic leukemia. Blood Cancer Discov. *1*, 82–95. https://doi.org/10.1158/2643-3230.BCD-19-0080.

Vaquerizas, J.M., Kummerfeld, S.K., Teichmann, S.A., and Luscombe, N.M. (2009). A census of human transcription factors: function, expression and evolution. Nat. Rev. Genet. *10*, 252–263. https://doi.org/10.1038/nrg2538.

Wainberg, M., Kamber, R.A., Balsubramani, A., Meyers, R.M., Sinnott-Armstrong, N., Hornburg, D., Jiang, L., Chan, J., Jian, R., Gu, M., et al. (2021). A genome-wide atlas of co-essential modules assigns function to uncharacterized genes. Nat. Genet. *53*, 638–649. https://doi.org/10.1038/s41588-021-00840-z.

Wang, H., Lee, C.H., Qi, C., Tailor, P., Feng, J., Abbasi, S., Atsumi, T., and Morse, H.C. (2008). IRF8 regulates B-cell lineage specification, commitment, and differentiation. Blood *112*, 4028–4038. https://doi.org/10.1182/blood-2008-01-129049.

Wang, T., Yu, H., Hughes, N.W., Liu, B., Kendirli, A., Klein, K., Chen, W.W., Lander, E.S., and Sabatini, D.M. (2017). Gene essentiality profiling reveals gene networks and synthetic lethal interactions with oncogenic ras. Cell *168*, 890–903.e15. https://doi.org/10.1016/j.cell.2017.01.013.

Wei, J., Wunderlich, M., Fox, C., Alvarez, S., Cigudosa, J.C., Wilhelm, J.S., Zheng, Y., Cancelas, J.A., Gu, Y., Jansen, M., et al. (2008). Microenvironment determines lineage fate in a human model of MLL-AF9 leukemia. Cancer Cell *13*, 483–495. https://doi.org/10.1016/j.ccr.2008.04.020.

Will, B., Vogler, T.O., Narayanagari, S., Bartholdy, B., Todorova, T.I., da Silva Ferreira, M., Chen, J., Yu, Y., Mayer, J., Barreyro, L., et al. (2015). Minimal PU.1 reduction induces a preleukemic state and promotes development of acute myeloid leukemia. Nat. Med. *21*, 1172–1181. https://doi.org/10.1038/nm.3936.

Wingelhofer, B., Maurer, B., Heyes, E.C., Cumaraswamy, A.A., Berger-Becvar, A., de Araujo, E.D., Orlova, A., Freund, P., Ruge, F., Park, J., et al. (2018). Pharmacologic inhibition of STAT5 in acute myeloid leukemia. Leukemia *32*, 1135–1146. https://doi.org/10.1038/s41375-017-0005-9.

Wunderlich, M., Mizukawa, B., Chou, F.-S., Sexton, C., Shrestha, M., Saunthararajah, Y., and Mulloy, J.C. (2013). AML cells are differentially sensitive to chemotherapy treatment in a human xenograft model. Blood *121*, e90–e97. https://doi.org/10.1182/blood-2012-10-464677.

Xu, K., and Zhao, Y.-C. (2016). MEF2D/Wnt/β-catenin pathway regulates the proliferation of gastric cancer cells and is regulated by microRNA-19. Tumour Biol. *37*, 9059–9069. https://doi.org/10.1007/s13277-015-4766-3.

Xu, Y., Milazzo, J.P., Somerville, T.D.D., Tarumoto, Y., Huang, Y.-H., Ostrander, E.L., Wilkinson, J.E., Challen, G.A., and Vakoc, C.R. (2018). A TFIID-SAGA perturbation that targets MYB and suppresses acute myeloid leukemia. Cancer Cell *33*, 13–28.e8. https://doi.org/10.1016/j.ccell.2017.12.002.

Yamanaka, R., Barlow, C., Lekstrom-Himes, J., Castilla, L.H., Liu, P.P., Eckhaus, M., Decker, T., Wynshaw-Boris, A., and Xanthopoulos, K.G. (1997). Impaired granulopoiesis, myelodysplasia, and early lethality in CCAAT/enhancer binding protein epsilon-deficient mice. Proc. Natl. Acad. Sci. USA *94*, 13187–13192. https://doi.org/10.1073/pnas.94.24.13187.

Young, R.A. (2011). Control of the embryonic stem cell state. Cell *144*, 940–954. https://doi.org/10.1016/j.cell.2011.01.032.

Yun, H., Narayan, N., Vohra, S., Giotopoulos, G., Mupo, A., Madrigal, P., Sasca, D., Lara-Astiaso, D., Horton, S.J., Agrawal-Singh, S., et al. (2021). Mutational synergy during leukemia induction remodels chromatin accessibility, histone modifications and three-dimensional DNA topology to alter gene expression. Nat. Genet. *53*, 1443–1455. https://doi.org/10.1038/s41588-021-00925-9.

Zhan, T., Rindtorff, N., and Boutros, M. (2017). Wnt signaling in cancer. Oncogene *36*, 1461–1473. https://doi.org/10.1038/onc.2016.304.

Zhang, S. (2008). The role of aberrant transcription factor in the progression of chronic myeloid leukemia. Leuk. Lymphoma *49*, 1463–1469. https://doi.org/10.1080/10428190802163305.

Zhang, D.E., Hohaus, S., Voso, M.T., Chen, H.M., Smith, L.T., Hetherington, C.J., and Tenen, D.G. (1996). Function of PU.1 (Spi-1), C/EBP, and AML1 in early myelopoiesis: regulation of multiple myeloid CSF receptor promoters. Curr. Top. Microbiol. Immunol. *211*, 137–147. https://doi.org/10.1007/978-3-642-85232-9_14.

Zhang, L., Li, Z., Yan, J., Pradhan, P., Corpora, T., Cheney, M.D., Bravo, J., Warren, A.J., Bushweller, J.H., and Speck, N.A. (2003). Mutagenesis of the Runt domain defines two energetic hot spots for heterodimerization with the core binding factor beta subunit. J. Biol. Chem. *278*, 33097–33104. https://doi.org/10.1074/jbc.M303972200.

Zhang, Y., Liu, T., Meyer, C.A., Eeckhoute, J., Johnson, D.S., Bernstein, B.E., Nusbaum, C., Myers, R.M., Brown, M., Li, W., and Liu, X.S. (2008). Model-based analysis of ChIP-seq (MACS). Genome Biol. *9*, R137. https://doi.org/10.1186/gb-2008-9-9-r137.

Zhao, L., Zhang, P., Galbo, P.M., Zhou, X., Aryal, S., Qiu, S., Zhang, H., Zhou, Y., Li, C., Zheng, D., et al. (2021). Transcription factor MEF2D is required for the maintenance of MLL-rearranged acute myeloid leukemia. Blood Adv. *5*, 4727–4740. 2021004469. https://doi.org/10.1182/bloodadvances.2021004469.

Zhao, X., Chen, A., Yan, X., Zhang, Y., He, F., Hayashi, Y., Dong, Y., Rao, Y., Li, B., Conway, R.M., et al. (2014). Downregulation of RUNX1/CBFβ by MLL fusion proteins enhances hematopoietic stem cell self-renewal. Blood *123*, 1729–1738. https://doi.org/10.1182/blood-2013-03-489575.

Zhou, J., Wu, J., Li, B., Liu, D., Yu, J., Yan, X., Zheng, S., Wang, J., Zhang, L., Zhang, L., et al. (2014). PU.1 is essential for MLL leukemia partially via crosstalk with the MEIS/HOX pathway. Leukemia *28*, 1436–1448. https://doi.org/10.1038/leu.2013.384.

Zhu, L.J., Gazin, C., Lawson, N.D., Pagès, H., Lin, S.M., Lapointe, D.S., and Green, M.R. (2010). ChIPpeakAnno: a bioconductor package to annotate ChIP-seq and ChIP-chip data. BMC Bioinf. *11*, 237. https://doi.org/10.1186/1471-2105-11-237.

Zuber, J., Rappaport, A.R., Luo, W., Wang, E., Chen, C., Vaseva, A.V., Shi, J., Weissmueller, S., Fellmann, C., Fellman, C., et al. (2011a). An integrated approach to dissecting oncogene addiction implicates a Myb-coordinated self-renewal program as essential for leukemia maintenance. Genes Dev. *25*, 1628–1640. https://doi.org/10.1101/gad.17269211.

Zuber, J., Shi, J., Wang, E., Rappaport, A.R., Herrmann, H., Sison, E.A., Magoon, D., Qi, J., Blatt, K., Wunderlich, M., et al. (2011b). RNAi screen identifies Brd4 as a therapeutic target in acute myeloid leukaemia. Nature *478*, 524–528. https://doi.org/10.1038/nature10334.

STAR★METHODS

KEY RESOURCES TABLE

REAGENT or RESOURCE	SOURCE	IDENTIFIER
Antibodies		
Rabbit polyclonal anti-MEF2D	Abcam	Product #: ab32845
Rabbit polyclonal anti-MEF2D	Bethyl Laboratories	Product #: A303-522A
Rabbit monoclonal anti-IRF8	Abcam	Product #ab207418, Lot #GR3271578-1
Rabbit polyclonal anti-PU.1	Cell Signaling Technology	Product #: 2266
Monoclonal ANTI-FLAG® M2 antibody	Sigma-Aldrich	Cat# F1804; RRID: AB_262044
Mouse monoclonal anti-HA (clone 12CA5)	Laboratory of Gerd Blobel	N/A
Rabbit monoclonal anti-GAPDH	Cell Signalling Technology	Product #14C10
Rabbit polyclonal anti-FKBP12 antibody	Abcam	Cat# ab24373
Mouse monoclonal anti-VINCULIN	Santa Cruz Biotechnology	Product #: sc-73614
Rabbit polyclonal anti-H3K27ac	Abcam	Cat# ab4729; RRID: AB_211829
Rabbit polyclonal anti-H3K4me1	Abcam	Product #: ab8895
PerCP anti-mouse CD45 Antibody	Biolegend	Cat# 103130
IgG from rabbit serum	Sigma-Aldrich	Cat#: I8140
Alexa Fluor® 680 Goat anti-mouse IgG (H + L)	Life Technologies	Product #A21058, Lot #1692967
IRDye® 800CW Goat anti-Rabbit IgG Secondary Antibody	LI-COR	Product #926-3221, Lot #C81210-05
Chemicals, peptides, and recombinant proteins		
Halt Protease & Phosphatase Inhibitor Cocktail, EDTA-free (100x)	Thermo Fisher Scientific	Ref #78441, Lot #UF284419
Glycogen	Roche	Ref #10901393001, Lot #11651224
SuperScript II Reverse Transcriptase	Thermo Fisher Scientific	Cat# 18064014
AMPure XP	Beckman Coulter	A63880
Penicillin/Streptomycin	Thermo Fisher Scientific	15140122
Proteinase K	New England Biolabs	P8107S
Puromycin dihydrochloride	Sigma-Aldrich	P8833
Blasticidin	Invitrogen	R21001
Geneticin Selective Antibiotic (G418 Sulfate)	Thermo Fisher Scientific	10131035
Polyethylenimine, PEI	Polysciences, INC	23966
OPTI-MEM	Thermo Fisher Scientific	31985070
Hexadimethrine Bromide, Polybrene	Sigma-Aldrich	H9268
Dynabeads Protein A	Thermo Fisher Scientific	Ref #10002D, Lot #00651865
TRIzol Reagent	Thermo Fisher Scientific	15596018
T4 DNA polymerase	New England Biolabs	M0203L
T4 polynucleotide kinase	New England Biolabs	M0201L
Agarose, Standard, Low Electroendosmosis (EEO)	Avantor	A426-07
2-Mercaptoethanol	Sigma-Aldrich	M6250
30% Acrylamide/Bis Solution, 37.5:1	Bio-Rad	1610158
2XLaemmli Sample Buffer	Bio-Rad	1610737
Dimethyl Sulfoxide	Sigma-Aldrich	D2650
Concanavalin A–coated Magnetic Beads	Bangs Laboratories	BP531

(*Continued on next page*)

Continued

REAGENT or RESOURCE	SOURCE	IDENTIFIER
Digitonin	EMD Millipore	300410
Spermidine	Sigma-Aldrich	S2501
dTAG-47	This study	N/A
pA-MN	This study	N/A
Spike-in DNA	Laboratory of Steven Henikoff	N/A
Roche Complete Protease Inhibitor (EDTA-free) tablets	Sigma-Aldrich	5056489001
DNA Polymerase I, Large (Klenow) Fragment	New England Biolabs	M0210
Formaldehyde 37% Solution	Avantor	2106-01
RNase A	Thermo Fisher Scientific	EN0531
Phenol/Chloroform/Isoamyl Alcohol	Thermo Fisher Scientific	BP1752I400
NP-40 (Igepal CA-630)	Sigma	I8896
rmIL3	Peprotech	213-13
rmIL6	Peprotech	216-16
rmSCF	Peprotech	250-03
Methylcellulose-based Medium with Recombinant for Mouse	STEMCELL technologies	M3434
Critical commercial assays		
CellTiter-Glo® Luminescent Cell Viability Assay	Promega	G7570
In-Fusion HD Cloning Kit	Takara Bio	638909
2x Phusion Master Mix	Thermo Scientific	F-548
Direct-zol RNA Miniprep Plus	Zymo Research	R2072
QuantSeq 3′ mRNA-seq Library Prep Kit for Illumina	Lexogen	015.96
Dead Cell Removal Kit	Miltenyi Biotec	130-090-101
Agilent High Sensitivity DNA Kit	Agilent	5067-4626
QIAquick PCR Purification Kit	QIAGEN	28104
Quick-DNA Miniprep Kit	ZYMO Research	D3025
NucleoSpin Gel and PCR Clean-up Mini Kit	Macherey-Nagel	740609.250
Aligent RNA 6000 Nano Kit	Aligent	5067-1511
NEBNext® Library Quant Kit for Illumina	NEB	E7630
NEBNext® Ultra™ II RNA Library Prep Kit for Illumina®	NEB	E7770
NEBNext® Poly(A) mRNA Magnetic Isolation Module	NEB	E7490
Deposited data		
RNA-seq, ChIP-seq and CUT&RUN data	This study	GSE186132
ChIP-seq	(Tarumoto et al., 2018)	GSE109493
ChIP-seq	(Mohaghegh et al., 2019)	GSE123872
ChIP-seq	(Poppe et al., 2017)	GSE89212
ChIP-seq and CUT&RUN	(Krivtsov et al., 2019)	GSE127508
ChIP-seq	(Rathert et al., 2015)	GSE63782
RNA-seq and ATAC-seq	(Corces et al., 2016)	GSE75384
RNA-seq	(Cao et al., 2021)	GSE157249
ChIP-seq and CUT&RUN	(Cao et al., 2021)	GSE157636
ChIP-seq	(Minderjahn et al., 2020)	GSE128834
RNA-seq	(Secker et al., 2020)	GSE148714
RNA-seq	(Barabé et al., 2017)	GSE71800
Dnase I-seq	(Assi et al., 2019)	GSE108316

(*Continued on next page*)

Continued

REAGENT or RESOURCE	SOURCE	IDENTIFIER
Experimental models: Cell lines		
Human: MOLM-13	DSMZ	ACC-554
Human: MV4-11	ATCC	CRL-9591
Human: THP1	ATCC	TIB-202
Human: HEL	ATCC	TIB-180
Human: OCI-AML3	DSMZ	ACC-582
Human: U937	ATCC	CRL-1593.2
Human: K562	ATCC	CCL-243
Human: JURKAT	ATCC	TIB-152
Human: REH	ATCC	CRL-8286
Human: HEK293T	ATCC	CRL-3216
Human: A549	ATCC	CCL-185
Human : HUH7	JCRB	JCRB0403
Human: A375	ATCC	CRL-1619
Human: OCI-AML5	Laboratory of James D. Griffin	NA
Human: MA9-ITD	(Wei et al., 2008; Wunderlich et al., 2013)	NA
Human: MA9-RAS	(Wei et al., 2008; Wunderlich et al., 2013)	NA
Experimental models: Organisms/strains		
Constitutive-Cas9-GFP	JAX	Stock No: 026179
Oligonucleotides		
sgRNA sequence see Table S2	This study	N/A
qPCR primers see Table S3	This study	N/A
Recombinant DNA		
LentiV_*neo*_empty	(Tarumoto et al., 2018)	Addgene: 108101
LentiV_*neo*_SFFV_MEF2D_short	This study	N/A
LentiV_*neo*_SFFV_MEF2D_long	This study	N/A
LentiV_*neo*_IRF8	(Cao et al., 2021)	N/A
LentiV_Cas9_puro	(Tarumoto et al., 2018)	N/A
LRG(Lenti_sgRNA_EFS_GFP)	(Tarumoto et al., 2018)	Addgene:65656
LRG2.1	(Tarumoto et al., 2018)	Addgene:108098
LRcherry2.1	(Tarumoto et al., 2018)	Addgene:108099
pSL21-mCherry	(Chen et al., 2021)	Addgene:164410
pRG212	(Gier et al., 2020)	Addgene: 149722
Software and algorithms		
Bowtie2 v2.3.5	(Langmead and Salzberg, 2012)	http://bowtie-bio.sourceforge.net/bowtie2/index.shtml
BEDtools v2.28.0	(Quinlan and Hall, 2010)	http://bedtools.readthedocs.io/en/latest/
Samtools v1.1	(Li et al., 2009)	http://samtools.sourceforge.net
HOMER v4	(Heinz et al., 2010)	http://homer.ucsd.edu/homer/
bcl2fastq Conversion Software, v2.17	Illumina, Inc.	https://support.illumina.com/sequencing/sequencing_software/bcl2fastq-conversion-software.html
MACS2 v2.1	(Zhang et al., 2008)	https://github.com/taoliu/MACS

(*Continued on next page*)

Continued

REAGENT or RESOURCE	SOURCE	IDENTIFIER
UCSC Genome Browser	UCSC	http://genome.ucsc.edu/
deepTools	(Ramírez et al., 2016)	https://deeptools.readthedocs.io/en/develop/
Picard tools v1.96	Broad Institute	https://github.com/broadinstitute/picard
STAR v2.5.2	(Dobin et al., 2013)	https://github.com/alexdobin/STAR
HTSeq, htseq-count, v0.6.1pL	(Anders et al., 2015)	https://htseq.readthedocs.io/en/release_0.11.1/
R Bioconductor DESeq2 package v1.14.1	(Love et al., 2014)	https://bioconductor.org/packages/release/bioc/html/DESeq2.html
MSigDB v6.1	(Liberzon et al., 2015)	http://software.broadinstitute.org/gsea/msigdb/index.jsp
Cufflinks	(Trapnell et al., 2013)	http://cole-trapnell-lab.github.io/cufflinks/cuffdiff/
deepTools	(Ramírez et al., 2016)	https://deeptools.readthedocs.io/en/develop/index.html
IGVtools, 2.4.10	Broad Institute	https://software.broadinstitute.org/software/igv/igvtools
GraphPad Prism 7	GraphPad Software	N/A

RESOURCE AVAILABILITY

Lead contact

Further information and reasonable requests for resources and reagents should be directed to and will be fulfilled by the Lead Contact, Junwei Shi (jushi@upenn.edu).

Materials availability

All plasmids will be deposited to Addgene for public requests (Addgene numbers in the key resources table).

Data and code availability

The accession number for the RNA-seq, ChIP-seq and CUT&RUN, generated in this study is: GSE186132. Data reported in this paper will be shared by the lead contact upon reasonable request. This paper does not generate original code. Any additional information required to reanalyze the data reported in this paper is available from the lead contact upon reasonable request.

EXPERIMENTAL MODEL AND SUBJECT DETAILS

Cell lines

HEK293T, A375 and HUH7 cell lines were cultured in DMEM (Corning) supplemented with 10% Bovine Calf Serum (FCS) and 1% Penicillin/Streptomycin. MOLM-13, MV4-11, THP-1, OCI-AML3, K562, U937, HEL, REH, OPM1 and JURKAT cell lines were cultured in RPMI-1640 (Gibco) supplemented with 10% FCS and 1% Penicillin/Streptomycin. MA9-ITD and MA9-RAS cell lines were cultured in RPMI-1640 supplemented with 10% Bovine Fetal Serum (FBS) and 1% Penicillin/Streptomycin. The OCI-AML5 cell line was cultured in alpha-MEM supplemented with 20% FBS, 1% Penicillin/Streptomycin and 10 ng/mL GM-CSF. All cells were maintained at 37°C with 5% CO_2.

Primary AML samples

The protocols used for this study were approved by the University Pennsylvania's institutional review board. The primary AML samples were obtained from the Stem Cell and Xenograft Core Facility at The Perelman School of Medicine at the University of Pennsylvania. Specimens were used after informed consent in accordance with the Declaration of Helsinki. The primary AML samples were frozen in FCS and 10% DMSO in liquid nitrogen until used. Patient clinical info is included in Table S4.

Mouse models

Around 12–16 weekold male *Gt(ROSA)*$^{26Sortm1.1(CAG-cas9*,-EGFP)Fezh}$ mice (constitutively expressing Cas9-GFP mice) were used in this study and purchased from the Jackson Laboratory. All animal protocols were approved by the Institutional Animal Care and Use Committee at the Children's Hospital of Philadelphia.

METHOD DETAILS

sgRNA and plasmid cloning

Cancer cell lines with stable Cas9 expression used in this study were generated via lentiviral transduction of spCas9 expression vector (Addgene: 108,100) and MOLM-13 cell line with stable Cas12a expression were generated via transduction of the AsCas12a lentiviral expression vector (Addgene: 149,723), followed by 1–2 μg/mL puromycin selection for 1 week. For dCas9-KRAB-mediated *MEF2D* regulatory element inhibition, sgRNAs were designed to target the TSS of MEF2D (NM_005920) and the proximal H3K27ac-enriched regions. For the AsCas12a-mediated deletion of the MEF2D and IRF8 regulatory elements, sgRNAs were designed to delete the region surrounding the identified enhancer elements. The sense and antisense DNA oligos of all the human sgRNAs were annealed and phosphorylated using T4 PNK (NEB M0201S). For human Cas9 sgRNAs, the oligos were ligated with T4 DNA ligase (NEB B0202S) to either BsmBI digested LRG2.1 plasmid (Addgene: 108,098) or LRCherry2.1 (Addgene: 108,099) backbones co-expressing a GFP or Cherry fluorescent tag, respectively. For murine Cas9 sgRNAs, the oligos were ligated into the BbsI digested pSL21-mCherry (Addgene:164,410) vector. The AsCas12a crRNAs were ligated with T4 DNA ligase (NEB B0202S) to an AsCas12a crRNA vector co-expressing GFP and neomycin selection gene (Addgene: 149,722). All sgRNA/crRNA sequences are listed in Table S2.

MEF2D cDNA (NM_001271629 and NM_005920) were obtained from the MOLM-13 cDNA and subcloned into a modified LentiV_*Neo* lentiviral expression vector (Addgene: 108,101) with an EFS promoter swapped to SFFV using the In-Fusion cloning system (Takara Bio). PCR mutagenesis and In-Fusion cloning were used to introduce synonymous mutations CGA → AGG (R), ATC → ATT (I), ACC → ACT (T), GAC → GAT (D), GAG → GAA (E) and CGG → CGT (R) into the MEF2D cDNA to generate a sgRNA-resistant construct.

Virus production and transduction

For lentivirus production, HEK293T cells were co-transfected with the plasmid DNA of interest, lentiviral packaging plasmids pPAX2 and VSVG, and the cationic polymer reagent Polyethyleneimine (PEI). To produce lentivirus in 6-well plates, 5 μg of the DNA, 2.5 μg of VSVG, 3.5 μg pPAX2, 1 mg/mL PEI and 500 μL OPTI-MEM were used. To produce lentivirus in 10-cm plates, 10 μg of the DNA, 5 μg of VSVG, 7.5 μg pPAX2, 1 mg/mL PEI and 1 mL OPTI-MEM were used. The components were incubated for 18 min at room temperature and transfected into >95% confluent HEK293T cells. The HEK293T cells were incubated at 37°C with 5% CO_2 for ~6–8 h before aspiration of theold media and replenishment with fresh DMEM. Supernatant containing lentivirus was collected at 24, 48 and 72h post-transfection and filtered using a 0.45 μm PVDF membrane (Millex-HV). For retrovirus production, retroviruses were produced in 10-cm plates using 10 μg plasmid, 2 μg pCL-Eco, 2 μg VSVG, 40 μL PEI and 1 mL OPTI-MEM. Virus was collected at 24 and 48 h post-transfection, pooled together and filtered by the 0.45μm filter.

To lentivirally/retrovirally transduce the cells, the cells were combined with 4 μL/mL polybrene (2 mg/mL) and virus, followed by spin-infection at 650 x g for 25 min at room temperature. Media was replaced on 12 h postinfection, administered with appropriate antibiotic selection if needed (1 mg/mL G418).

Competition-based cell proliferation assay

To validate the effect of knockout on proliferation, cancer cell lines stably expressing spCas9 were transduced with LRG2.1 or LRcherry2.1 sgRNAs. The transduction of the sgRNAs were measured based on the fluorescence detected using Guava Easycyte HT Instrument (Millipore). For single gene validation, percentage of the GFP + or mCherry + transduced cells were measured on Day 3 post-infection and measured every 3 days for 15–21 days. The GFP% was normalized based on Day 3. For dual CRISPR-based disruption, cells were co-transduced with GFP and mCherry-tagged gRNAs and measured using the Guava Easycyte HT Instrument (Millipore) from day 3 post-infection. The percentage of transduction efficiency of non-transduced, GFP+, Cherry+, GFP+/Cherry+ were measured based on their ratios in the mixed population of cells.

Immunoblotting

Cells were counted using the Guava Easycyte HT Instrument (Millipore) and washed with 1X PBS. Proteins were lysed using a 26-gauge x 5/8-inch needle and 1 mL syringe (BD) in Laemmli sample buffer (Bio-Rad) containing 3% β-Mercaptoethanol. Extracted protein-containing lysates were boiled at 95°C for 7 min. Extracts were loaded onto 10% polyacrylamide gels and transferred to 0.45 μm nitrocellulose membranes. The membrane was blocked with 5% milk in TBST at room temperature in a shaking platform, followed by 1° antibody (MEF2D: Bethyl #A303-522A, PU.1: CST #2266, Vinculin: Santa Cruz #sc-73614, GAPDH: CST #5014, IRF8: Abcam #ab207418) diluted in 5% milk in TBST overnight incubation in a shaking platform at 4°C. Membrane was washed with PBST for 3 × 5 min. The 2° antibody solution was prepared with 1% secondary antibody and 1X LICOR blocking buffer in PBST. The membrane was incubated in the dark with the 2° antibody solution for 1h and imaged using the Odyssey CLx (LI-COR) imager. The image was quantified in Image™ Studio Lite.

Colony formation assay

Bone marrow cells were isolated from the femurs of Cas9-expressing mice (JAX). ACK buffer (150 mM NH_4Cl, 10 mM $KHCO_3$, 0.1 mM EDTA) was used to lyse the erythroid cells, and the remaining BM cells were cultured in IMDM media supplemented with 15% FBS, 1% Penicillin/Streptomycin, 10 ng/mL rmIL-6, 10 ng/mL rmIL-3 and 20 ng/mL rmSCF. BM cells were transduced with sgRNA in pSL21-mCherry retroviral vectors as described above. On day 2 post-infection, GFP+/mCherry + double-positive cells were sorted, and 25,000 cells were seeded into MethoCult GF M3434 media containing murine cytokines. Following 10 days of incubation, differentiated colonies were counted according to the manufacturer's protocols, including burst-forming unit-erythroid (BFU-E), macrophage (CFU-GM), CFU-granulocyte and CFU-granulocyte, erythrocyte, macrophage, megakaryocyte (CFU-GEMM).

RNA-seq

MOLM-13 cells were harvested on day 5 post-infection of sgRNA, MV4; 11 and K562 cells were harvested on day 4 post-infection, and THP-1 cells were harvested on day 10 post-infection. Approximately 1–5 million cells transduced with sgRNAs were collected and lysed in Trizol (Invitrogen). Total RNA was isolated using the Direct-zol RNA Miniprep Plus kit (ZYMO) with DNAse I treatment, followed by RNA quality check using the RNA Nano 6000 Bioanalyzer kit (Agilent). RNA-seq libraries were prepared using the QuantSeq 3′ FWD mRNA-seq Library Prep Kit (Lexogen) with 0.5–2 μg of total RNA inputs following the manufacturer's protocol. Library quality was assessed using the High Sensitivity Bioanalyzer kit (Agilent) and libraries were sequenced on the Nextseq 500 platform with 75 bp single-end reads.

Primary human samples were first washed with the Dead Cell Removal Kit (MACS) to remove dead cells. Total RNA was isolated from 1 to 3 million cells using Direct-zol RNA Miniprep Plus kit (ZYMO), followed by construction of the RNA-seq library using NEBNext Ultra II RNA Library Prep Kit for Illumina. One μg of total RNA was poly-A selected followed by fragmentation using the NEBNext PolyA(A) mRNA Magnetic Isolation module. The selected RNAs were subjected to a first and second strand cDNA synthesis. The libraries were end-repaired and linked with Illumina adaptors. The libraries were PCR amplified using 8 cycles, followed by sequencing using the Nextseq 500 platform with 75bp single-end reads or 2 × 42 paired-end reads. Sequencing data information was provided in Table S6.

ChIP-sequencing and ChIP-qPCR

For targeted degradation, MOLM13-dIRF8 (cells derived from MOLM13 expressing degradable IRF8 via dTAG system with endogenous IRF8 depletion) cells (Cao et al., 2021) were treated with either DMSO or 500 nM dTAG-47 compound and collected at 4 and 24h timepoints. For all the experiments, cells were collected in culture media, and crosslinked in 1% formaldehyde for 20 min at room temperature, and the reaction was sequestered with 0.125M Glycine in PBS for 10 min. The crosslinked cells were spun down, washed with PBS and frozen in −80°C until use. Ten million cells were used for H3K27ac and H3K4me1, and 50 million cells for the SPI1, respectively. Cell pellets were lysed in cell lysis buffer (10mM Tris pH 8.0, 10 mM NaCl, 0.2% NP-40) with protease inhibitor (Roche) and incubated for 15 min on ice. The cells were spun down for 30 s at 4,200 RPM and the buffer was removed. The cells were resuspended in 1mL nuclear lysis buffer (50 mM Tris pH 8.0, 10 mM EDTA, 1% SDS) per 10 million cells, followed by a 10 min incubation on ice. The cells were sonicated with a bioruptor for 5 min at 4°C and spun down at max speed for 15 min at 4°C. Supernatants containing fragmented chromatins were collected, diluted

with 7mL IP dilution buffer (20 mM Tris pH 8.0, 2 mM EDTA, 50 mM NaCl, 1% Triton X-100, 0.01% SDS) per 10 million cells, and applied with respective antibodies (PU.1: 10 μg, CST#2266; H3K27ac: 2 μg, #ab4729, H3K4me1: 2μg, #ab8895). For each antibody, 30 μL of protein A magnetic beads (Invitrogen) were applied after washing with 0.5% BSA in TBS for 3 times and blocked at 4°C on a rotor for 2h. The mixture was incubated overnight at 4°C in rotation. The beads were washed once with IP wash I buffer (20 mM Tris pH 8.0, 2 mM EDTA, 50 mM NaCl, 1% Triton X-100, 0.01% SDS), twice with high salt buffer (20 mM Tris pH 8.0, 2 mM EDTA, 500 mM NaCl, 1% Triton X-100, 0.01% SDS), once with IP wash 2 buffer (10 mM Tris pH 8.0, 1 mM EDTA, 0.25 M LiCl, 1% NP-40, 1% sodium deoxycholate), and twice with 1xTE. The beads were incubated with 200 μL elution buffer (50mM Tris 8.0.10mM EDTA, 1%SDS), vortexed 3x for 5s, followed by shaking at 950 RPM at 65°C for 15 min. Supernatants were collected and reverse crosslinking was performed in 0.25M NaCl at 65°C overnight. non-DNA content was eliminated with 2 μL RNase A for 1hat 37°C, followed by 0.2 mg/mL Proteinase K for 2hat 42°C. ChIP DNA was purified using QIAquick PCR purification kit according to manufacturer's instructions, and eluted with 40 μL water. ChIP-seq libraries were constructed using NEBNext Ultra II DNA Library Prep Kit for Illumina (E7645L) and the optimal cycle numbers were determined by NEBNext Library Quant Kit for Illumina (E7630L). Library quality was assessed using the high sensitivity Bioanalyzer kit (Agilent) and libraries were pooled and single-end sequenced for 75 bp on the Nextseq 500 platform. For ChIP-qPCR, PU.1 peak loci with or without IRF8 binding, and H3K27ac/H3K4me1-enriched regions obtained from ChIP-seq were selected. ChIP DNA was quantified using the ViiA 7 Real-Time PCR System (Applied Biosystems) with Power SYBR Green Master Mix (Thermo Fisher). A series of input dilution was used for normalization. qPCR Primer sequences and their chromosomal coordinates used for ChIP-qPCR are included in Table S3. Sequencing data information was provided in Table S6.

CUT&RUN and CUT&RUN qPCR

CUT&RUN experiments were slightly modified from a previous protocol (Cao et al., 2021; Skene et al., 2018). Concanavalin A-coated beads were washed with Binding buffer (20 mM HEPES-KOH, 10 mM KCl, 1 mM NaCl and 1 mM $MnCl_2$) prior to use. For MOLM-13 cells, 2×10^6 live cells were collected, and an extra 2×10^6 cells were harvested and saved as input in CUT&RUN qPCR. For primary patient cells, 5×10^5 cells were purified from the Dead Cell Removal kit (MACS) before use. Cells were washed twice in Wash buffer (150 mM NaCl, 20 mM HEPES-KOH pH 7.9, 0.5 mM Spermidine and protease inhibitor cocktail), and incubated in 1mL of Wash buffer containing 20 μL of Concanavalin A-coated beads for 5–10 min with rotation at room temperature. Cell-attached beads were then resuspended with 300 μL Antibody buffer (Wash buffer with 0.05% Digitonin and 2mM EDTA) in combination with 20 μL MEF2D antibody (Abcam, #ab32845), 2μL of H3K27ac antibody (Abcam #ab4729) or 2 μL IgG overnight at 4°C with rotation. Based were washed once with Dig-wash buffer (Wash buffer with 0.05% Digitonin) and resuspended in 300 μL Dig-wash buffer with 700 ng/mL pA-MN purified protein at 4°C for 1 h with rotation. Beads were then washed twice with Dig-wash buffer, resuspended in Dig-wash buffer and chilled on a heat block on ice. Chromatin digestion was conducted in the presence of $CaCl_2$ for 30 min and sequestered with an equal volume of 2x STOP solution (340 mM NaCl, 20 mM EDTA, 50 μg/mL RNase A, 4 mM EGTA, 0.02% Digitonin, 50 μg/mL Glycogen and 2 pg/mL heterogeneous spike-in DNA) at 37°C for 10 min. The supernatant was collected, and DNA and the input samples were subjected to Phenol-Chloro-form extraction. For CUT&RUN qPCR, the MEF2D peak loci at the IRF8 enhancer region were used for qPCR analysis. Sequencing libraries were constructed with NEBNext Ultra II DNA Library Prep Kit for Illumina following a previously described method (Liu et al., 2018) for TF or the default method for histone marks. Adapters were diluted 50x and 10–12 cycles of PCR amplification were applied. Library quality was assessed using the high sensitivity Bioanalyzer kit (Agilent) and libraries were pooled and paired-end sequenced for 2 × 42bp on the Nextseq 500 platform. qPCR Primer sequences and their chromosomal coordinates used for CUT&RUN-qPCR are included in Table S3. Sequencing data information was provided in Table S6.

RT-PCR

Total RNA was isolated using the Direct-zol RNA Miniprep Plus Kit (ZYMO) with DNAse I treatment manufacturer protocol. Reverse transcription of isolated RNA to cDNA was performed using RevertAid Reverse Transcriptase (Thermo) supplemented with 20 U/μL Riboblock. RT-PCR of cDNA was performed with PowerSYBR Green PCR Master Mix (Thermo #4367659) on the ABI 7900HT standard real-time PCR machine. All ΔCt values were normalized based on GAPDH expression. All the RT primers are listed in Table S3.

Deletion of regulatory elements

To delete the genomic regions at potential *MEF2D* or *IRF8* enhancer elements bound by *IRF8* or *MEF2D*, respectively, we utilized the Cas12a system (Gier et al., 2020) to induce simultaneous double-strand breaks flanking the TF binding sites. To enhance deletion efficiency, we designed four crRNAs on CRISPick (Doench et al., 2016), two of which target the upstream and two for the downstream of the element, with at least a 40bp gap between each crRNA. The combinatorial crRNAs targeting the *IRF8* or *MEF2D* enhancer will result in a 540-680bp or 850-950bp deletion, respectively. A quadrupole crRNA combination for the ROSA locus was used as a negative control. The total 4 crRNAs were cloned in a crRNA array of the pRG212 lentiviral expression vector (Addgene: 149,722). MOLM-13 cells stably expressing AsCas12a were transduced with the designated array, followed by 4-day neomycin selection. Measurement of the GFP fluorescent tag using the Guava Easycyte HT Instrument (Millipore) was used for further validation of crRNA transduction and measurement of selection efficiency. To measure the efficiency of the enhancer deletion, gDNA was isolated using the Quick-DNA Miniprep Plus Kit (ZYMO) and genotyped. PCR products were run in 1% agarose gel and band intensities were measured using Image Lab (BioRad) with value normalized by product size. Percentage of enhancer deletion was calculated using normalized enhancer-deleted band intensity divided by sum of normalized enhancer-deleted and intact band intensity, multiplied by 100. To measure transcriptional changes upon enhancer deletion, total RNA was isolated using the Direct-zol RNA Miniprep Plus Kit (ZYMO), followed by RT-PCR. Genotyping primers were listed in Table S3.

Identification of leukemia-selective TF dependencies

Genome-wide "drop-out" CRISPR screen data were retrieved and analyzed on the DepMap portal (https://depmap.org/portal/) using the 21Q2 Public + Score CERES dataset containing perturbation effects of 17,645 genes in 990 cell lines. Briefly, CERES was calculated and scaled as previously described (Meyers et al., 2017), such that the median non-essential and common essential gene perturbation effects are 0 and -1, respectively. The pan-dependent genes were defined as those whose ranks in 90% of cell lines were above a given dependency cut-off. The cut-off value is determined by the central minimum in the 90th percentile lowest dependency line in the gene rank histogram (Dempster et al., 2019).

To identify potential leukemia-specific dependencies, CERES in 23 AML cell lines, 14 ALL cell lines and 7 CML cell lines (termed "in-group") were compared with the remaining cell lines (term "out-group") as previously described (Dharia et al., 2021). Briefly, t-statistics and log-odd ratios of differential CERES were calculated based on a fitted linear regression model. Effect size was determined by the difference between the CERES in the in-group and the out-group. Cancer subtype-biased dependencies were identified as those with a negative t-statistics and p value lower than 0.05. Common essential and non-essential genes were filtered out, and genes categorized as TF based on previous studies (Lambert et al., 2018; Lu et al., 2018; Vaquerizas et al., 2009) were used for further analysis. For analysis on TF dependencies in combination with their mRNA expression, RNA-seq datasets (Expression 21Q2 Public) in leukemia cell lines were downloaded on the DepMap portal, and pairwise Pearson correlation between CERES of one gene and mRNA expression (normalized to $\log_2$(TPM+1)) of the others were conducted in R. Hierarchical clustering on TF dependencies was performed with the *pheatmap* (https://rdrr.io/cran/pheatmap/) or *ComplexHeatmap* (Gu et al., 2016b) function in R.

RNA-seq analysis

Primary AML samples were aligned to hg19 using STAR Aligner (Dobin et al., 2013). For cell lines, RNA-seq analysis was performed on the Quantseq FWD 2.3.6 pipeline (Lexogen). Briefly, sequencing reads were aligned to hg38 using STAR Aligner (Dobin et al., 2013) with low quality reads and adaptor contamination removed. RPM-normalized track files (bigwig) were generated with the bedGraphToBigWig tool. Raw read counts were generated using HTseq-count (Anders et al., 2015). For CRISPR-mediated disruption samples, raw read counts >10 were retained. Differential gene expression analysis was performed using DE-Seq 1.30.1 (Love et al., 2014). GO and ORA analysis was performed on WebGestalt 2019 (Liao et al., 2019). GSEA analysis was performed in accord with the GSEA instruction (https://www.gsea-msigdb.org/gsea/index.jsp) with Molecular Signature Database v6.1 (MSigDB) (Liberzon et al., 2015) and custom gene signatures that are listed on Table S1.

ChIP-seq and CUT&RUN processing

For ChIP-seq and CUT&RUN analysis, reads were aligned to hg19 using Bowtie2 v2.3.5 (Langmead and Salzberg, 2012), following parameters as previously described (Skene et al., 2018):–local–very-sensitive-local–no-unal–no-mixed–no-discordant–phred33-I 10-X 700-k1-N1. Picard tools v1.96 (Broad Institute)

was applied to displace presumed PCR duplicates using the *MarkDuplicates* command. Bam files with uniquely mapped reads retained were generated using Samtools v1.1 (Li et al., 2009). Fragments between 40 and 1000 bp were kept. Blacklist regions defined by ENCODE, random chromosomes, and mitochondria were removed, and filtered bam files were used for further analysis. Reads per kilobase per million mapped reads (RPKM)-normalized bigwig files were created using deeptools bamCoverage (Ramírez et al., 2016) with parameters-bs 10–smoothLength 50–normalizedUsing RPKM–skipNAs in cell lines, or default parameters in primary patient cells to visualize binding signals. Bigwig files of replicates were pooled together using WiggleTools mean setting. Tracks were loaded to UCSC genome browser for visualization. Pearson correlation of replicates were calculated using deepTools multiBigwigSummary bins with binning size as 10,000. Correlation heatmap were plotted using deepTools plotCorrelation with default hierarchical clustering.

CUT&RUN and ChIP-Seq enriched signals were called using MACS v2.1 (Zhang et al., 2008) with adjusted p value threshold 0.01 unless indicated. Genes in proximity with peaks were annotated against the hg19 genome using annotatePeaks.pl from HOMER v4 (Heinz et al., 2010).

Peak overlap and shifting analysis

The Venn diagram of comparisons of the ChIP/CUT&RUN peaks was generated using Bioconductor package ChIPpeakAnno (Zhu et al., 2010) function findOverlappingPeaks with mapped gap equal to 500bp. To identify shifts of IRF8 and MEF2D overlapped binding regions, we first calculated genomic distance (with orientation) and absolute distance between IRF8 and MEF2D peak summits. The distance distribution follows an approximate normal distribution. We then defined lower 20% of the peaks as IRF8 left-shifted peaks and upper 20% as IRF8 right-shifted peaks over MEF2D. Heatmaps and metaplots were generated using deepTools plotHeatmap (Ramírez et al., 2016).

Peak overlap and differential analysis

The Venn diagram of the IRF8 and PU.1 peaks comparison was generated using Bioconductor package ChIPpeakAnno (Zhu et al., 2010) function findOverlappingPeaks with mapped gap equal to 500bp. Metaplot and signal heatmap of the unique and overlapped enriched regions were generated using deepTools computeMatrix and plotHeatmap. We further quantified PU.1 read counts under IRF8 and PU.1 enriched regions using deepTools multiBigwigSummary BED-file setting to quantify RPKM normalized bigwig files. Using the same method, we then extended 1000bp on both sides of the narrow peaks, and quantified RPKM read counts of histone marks H3K27ac and H3K4me1. Differential analysis between DMSO and dTAG were performed using DESeq2. Boxplot of log2FC results from DESeq2 were plotted using ggplot2.

QUANTIFICATION AND STATISTICAL ANALYSIS

Statistical analysis was performed on either Graphpad Prism 9 or R. For linear regression, statistical analysis (p value) was calculated using a two-tailed F-test. For RNA-seq, ChIP-seq, RT-PCR and proliferation assay, statistical parameters including p value, biological replicates, SEM and FDR are indicated directly on the figures or in the corresponding figure legends.